CARMA SUMMER SCHOOL - July 2011
Introduction to Millimeter Wavelength Interferometry

Melvyn Wright

Radio Astronomy Laboratory, University of California, Berkeley, CA 94720

July 11, 2011

Contents

1 INTRODUCTION

1.1 Radio Astronomy

- Radio astronomy is an observational science. We make images of the radio intensity

$$I(\mathbf{s}, \nu, polarization, time)$$

  Observations measure I with sufficient resolution in $\mathbf{s}, \nu, polarization, time$.
  Measure source characteristics with sufficient sensitivity for the science goals.

- What we actually measure is
$$I' = I * B + noise$$

  B is the instrumental response.
  additive *noise* from receivers, telescope, spillover and atmosphere.

- Data reduction is the process of obtaining I from our measurements, I'
  calibrate, and deconvolve the instrumental response to obtain I from I'.

- Data Analysis is interpreting what I means for astronomy.

- We need to know something about the sources of radio emission
    in order to design our telescopes and observations.

- Some of the 1st observations in a new waveband are usually surveys
    to determine the distribution and nature of the sources.
    Later observations study the details of individual sources, or classes of sources.

- Instrumentation, and observing techniques together
    define a matched filter to a set of possible observations
    to determine the characteristics of $I(\mathbf{s}, \nu, poln, time)$.

- Source selection: astronomy, frequency, size, resolution, brightness, polarization.
    Some observations are a good match to the instrument.
    Others are more difficult: "challenging", or "impossible".
    We design new instruments to match new science goals.
    CARMA is a "new" instrument, evolving to meet new science goals.

1.2 Millimeter wavelength Radio Sources

- Astronomy from Comets to Cosmology

    Emission mechanisms: thermal and non-thermal

- Thermal emission is in quasi-equilibrium with the physical temperature.

    Black body - planets, asteroids, quiet sun

    Dust - grey body: dust emissivity at millimeter wavelengths

    Molecular lines: rotational-vibrational transitions

    Star formation regions, molecular clouds, stellar envelopes, YSO, evolved stars

    Galactic structure: CO and isotopes, CS, HCN, HCO+....

    Spiral and Dwarf galaxies: structure, gas content, rotation curves

- Non-Thermal emission is not in equilibrium with the physical temperature.

    Relativistic electrons & magnetic fields, synchrotron radiation,

    inverse compton, masers, cyclo-synchrotron

      SN remnants

      Radio galaxies: hot spots

      Active galaxies: nuclei

      Quasars, Blazars, and Seyfert galaxies.

      Active sun: Solar flares.

      Masers: SiO, CH3OH

      Pulsars: steep spectrum, not important at millimeter wavelengths

      Comets: collisional (inner coma), and fluorescent excitation (Solar IR photons)

- Student Projects

    Is your project thermal or non-thermal emission ?

    what category in above list ?

1.3 Atmospheric windows

- Atmospheric windows at optical, IR, and radio frequencies

  Earthbound astronomical observations are possible through atmospheric windows
  at optical, IR, and radio frequencies.

  FIGURE 1. - Kraus - Radio Astronomy, 2nd ed.

  optical: $0.5 - 0.8\,\mu$m.

  IR: $1 - 1000\,\mu$m : bolometers, detector arrays.

  Radio: $350\,\mu$m -60 m : heterodyne receivers.

  λ mm: 0.3 mm -1 cm. (30 to 1000 GHz)

- Atmospheric windows are defined by O_2 and H_2O lines into a number of bands

  bounded by tropospheric absorption at high freq

  bounded by ionospheric absorption at low freq.

  FIGURE 2. - Terrestial Microwave window.

- Atmospheric absorption is strongly dependent on atmospheric water vapor, away from the strong absorption lines.

  scale height of water vapour is about 2 km.

  Observations at higher, drier sites have less absorption.
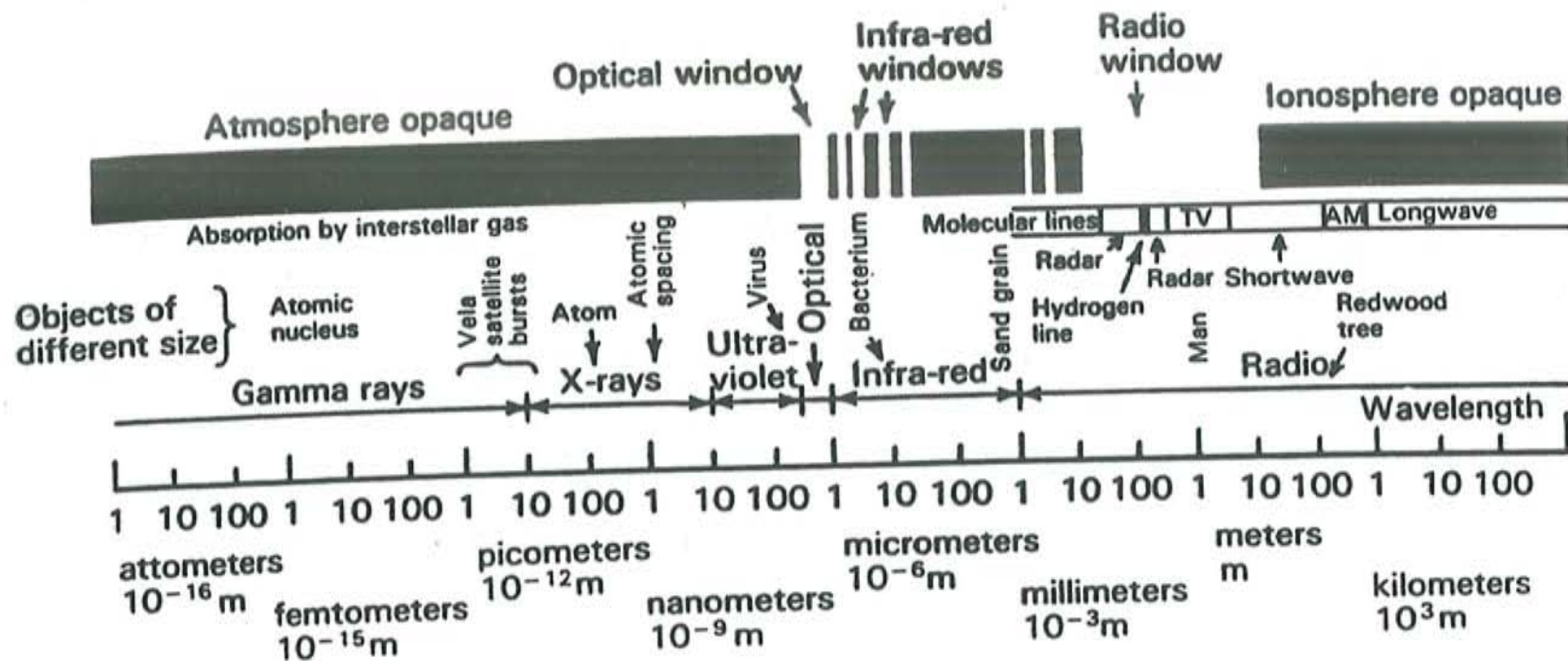
Fig. 1-1. Electromagnetic spectrum showing relative transparency of the earth's atmosphere and ionosphere.

Figure 1: Atmospheric windows at optical, IR, and radio frequencies. (Kraus - Radio Astronomy, 2nd ed.)

13
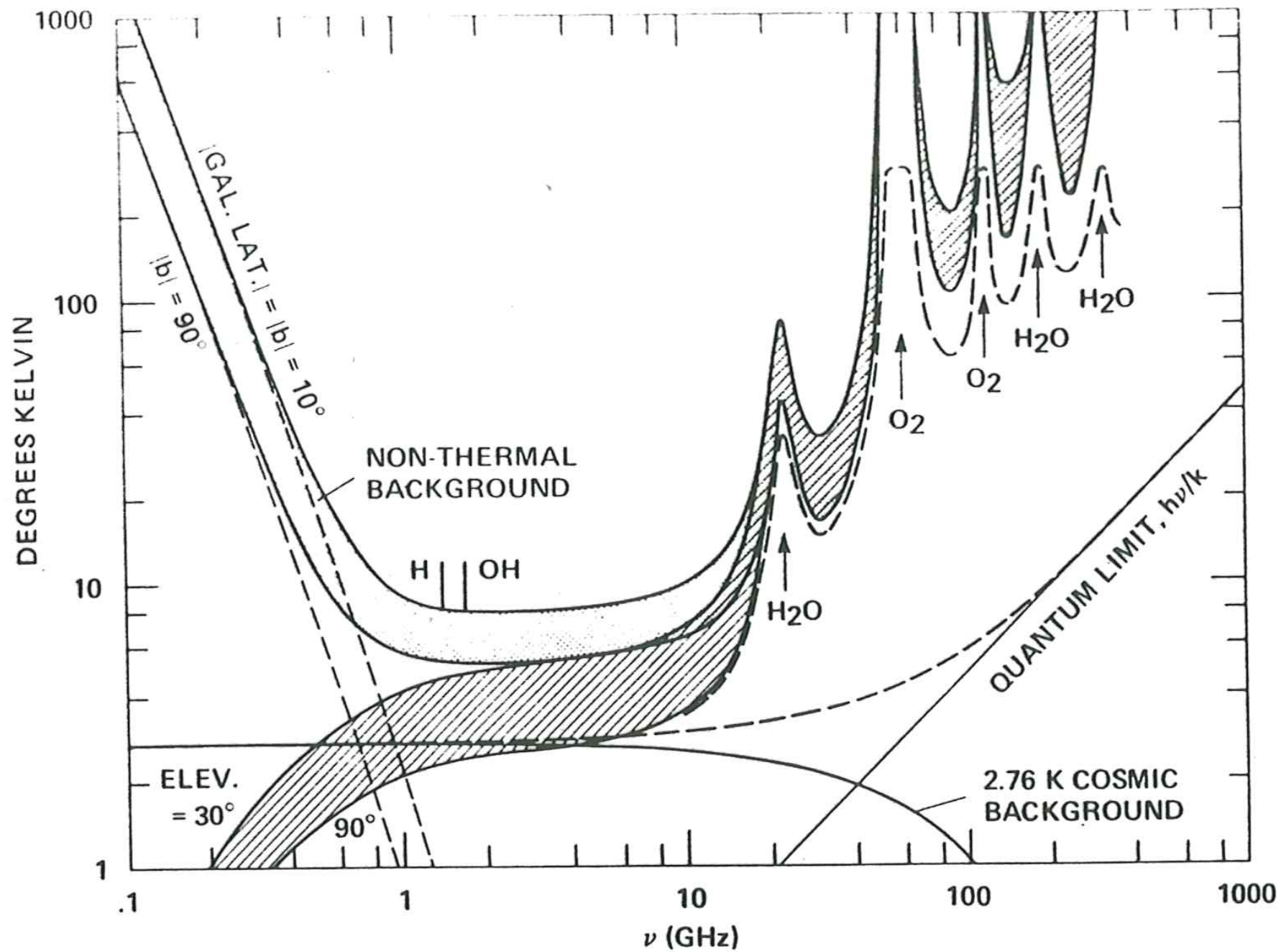
Figure 2.— Terrestrial microwave window.

- CARMA site characteristics.

    CARMA altitude is 2196 m.

    Typical "good" weather $\sim$ 4 mm precipitable water vapor; tau230 $\sim$ 0.27

    Best winter weather. $\sim$ 2 mm precipitable water vapor; tau230 $\sim$ 0.14

    Mauna Kea at 4 km altitude often less than 2 mm PWV; tau230 $\sim$ 0.12

    ALMA at 5 km altitude median PWV $\sim$ 1 mm ; tau230 $\sim$ 0.05

- CARMA observing bands.

    CARMA currently has receivers for 3 bands.

    1 mm band: $\sim$ 210 – 270 GHz

    3 mm band: $\sim$ 75 – 115 GHz

    1 cm band: $\sim$ 26 – 36 GHz

    atmospheric absorption is more serious in 1 mm band.

    advantages of a high, dry site are more obvious.

1.4   Intensity Units.

- Intensity units: $I(\mathbf{s}, \nu, polarization, time)$ watts m^{-2}str^{-1}Hz^{-1}

- Brightness Temperature

    for black body radiation

    $$I = \frac{2h\nu^3}{c^2} \frac{1}{(e^{h\nu/kT} - 1)}$$

    T is the **brightness temperature** of an equivalent black body radiator.

    $$h/k = 4.8 \ [GHz/100] \ K$$

- Rayleigh Jeans brightness temperature

    For $h\nu/kT << 1$,

    $$I = 2kT/\lambda^2 \ [1 - h\nu/2kT + ...]$$

    Rayleigh Jeans brightness temperature, T_b

    $$I = 2kT_b/\lambda^2$$

- Flux density

$$S = \int I \, \delta\Omega$$

1 Jansky $= 10^{-26}$ watts m^{-2} Hz^{-1}

e.g. Planet with uniform brightness temperature T_b,

$$S = 2kT_b/\lambda^2 \times \Delta\Omega$$

where $\Delta\Omega$ is the solid angle subtended by the planet.

- Brightness units: Kelvin, Jy/pixel, Jy/beam

1.5 Radio antennas: Collecting area and Aperture efficiency.

- **Collecting area $\sim D^2$**

  We build antennas to collect radio photons from astronomical sources.

  Radio astronomy antennas are not used to transmit radio waves - as in radar astronomy

  but it is often useful to think of antennas as transmitters.

  Amount of power we collect depends on the intensity, or brightness of radiation.

- Antenna has an effective collecting area $A(\mathbf{s})$; $\mathbf{s}$ is direction in sky.

  For an elemental flat collector, the effective collecting area $= \delta A \times cos(\theta)$

- Power we collect,

$$P[watts] = \int I(s) \; A(s) \; \delta\Omega \; \delta\nu \; \delta A$$

- Power collected by CARMA telescope from 1 Jy quasar ,

$$P[watts] = 0.5 \; S[watts \; m^{-2} \; \text{Hz}^{-1}] \times \Delta\nu[Hz] \times A[m^2]$$

$$P[watts] = 0.5 \; 10^{-26}[watts \; m^{-2} \; \text{Hz}^{-1}] \times 10^9[Hz] \times 100[m^2]$$

factor 0.5 is for 1 polarization

- Aperture efficiency

  effective collecting area = aperture efficiency × collecting area

  aperture illumination, the weighted sum of electric fields across the aperture

  feed legs, subreflector blockage, spillover.

- Surface accuracy

  Aperture efficiency also depends on surface roughness.

  E- fields are summed in phase across the aperture.

  Ruze losses reduce effective collecting area by a factor $\exp[(-(\frac{4\pi\sigma}{\lambda})^2]$

  Surface accuracy, $\sigma = \lambda/20$ corresponds to a Ruze loss factor 0.67.

- CARMA antennas

  Including thermal, pointing and focus errors, the overall RMS ~ 75 microns.

  at 3 mm wavelength, $exp(-(4\ \pi\ 75/3000)^2) \sim 0.91$

  at 1.3 mm wavelength, $exp(-(4\ \pi\ 75/1300)^2) \sim 0.59$

- Surface RMS ~ 30 microns, after correcting for pointing and focus errors.

  these are very good antennas at millimeter wavelengths.

1.6   Radio antennas: Angular Resolution

- **Resolution $\sim \lambda/D$**

- Antenna Voltage pattern

    antenna forms a weighted vector average of the E-field across the aperture

$$V(\mathbf{s}) = \int W(\mathbf{r}) \ E(\mathbf{r}) \ \exp(2\pi i \ \mathbf{r.s}/\lambda) \ \delta A$$

- Forward Gain: Sum the E-field across the aperture in phase in direction s_0.

$$\rightarrow\rightarrow\rightarrow\rightarrow\rightarrow\rightarrow \text{ in direction } s_0.$$

- Phase gradients across the aperture give an antenna resolution in direction.

    for radiation from other directions, phase gradients across the aperture reduce the vector sum of the E-field.

- Uniformly weighted rectangular aperture diameter D,

$$V(\mathbf{s}) = \int \ exp(2\pi i \ x \ sin(\theta)/\lambda) \ dx \quad [x = -D/2, D/2]$$

$$V(\theta) = \sin(\pi \ \theta \ D/\lambda)/(\pi \ \theta \ D/\lambda)$$

- Uniformly weighted circular aperture diameter D,

$$V(\theta) = 2J_1(\pi \ \theta \ D/\lambda)/(\pi \ \theta \ D/\lambda)$$

- Antenna power pattern
$$P(\mathbf{s}) = V(\mathbf{s}) \times V^{\star}(\mathbf{s})$$

  Primary beamwidth, FWHM $\sim 1.2 \ \lambda/D$

- Interferometer power pattern

  Primary beam for an interferometer is the cross power pattern.

  for each antenna pair (i, j),
$$P_{i,j}(\mathbf{s}) = V_i(\mathbf{s}) \times V_j^{\star}(\mathbf{s})$$

Figure 3–6. Optical systems for radio telescope reflectors. **(a)** Prime focus, **(b)** Cassegrain, **(c)** Off-axis Cassegrain, **(d)** Naysmith, **(e)** Beam waveguide, **(f)** Offset Cassegrain.
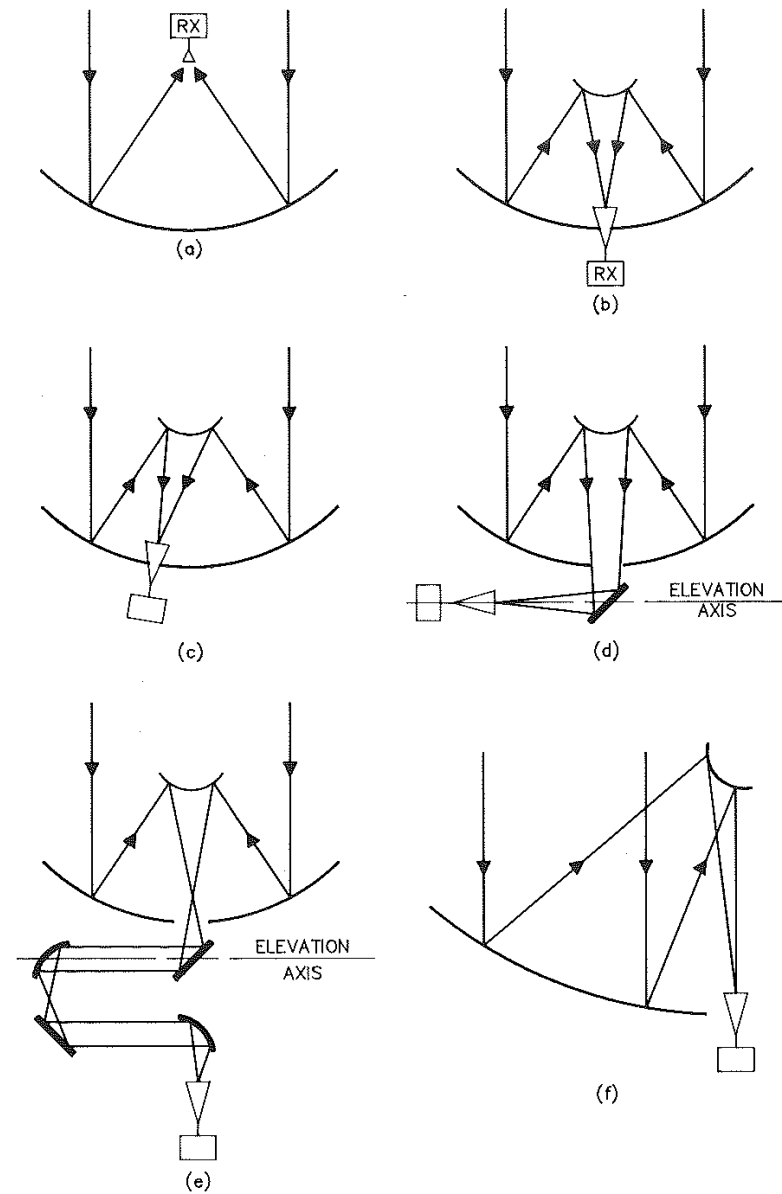
1.7 Radio Source Structure and Spatial Dynamic Range

- Early radio astronomy discovered radiation from the Galaxy, with unresolved maxima.

- Peaks named Cas A, Cygnus A, Sag A, Taurus A, Virgo A etc. Resolution $\sim$ 7 degrees.

   Small optical telescope $\lambda/D \sim 5 \ 10^{-5}/10$ cm. *Resolution* $\sim$ 1 arcsec.

   Arecibo: $\lambda/D \sim 6cm/300m \sim 36$ arcsec.

   Bonn: $\lambda/D \sim 1cm/100m \sim 20$ arcsec.

   IRAM 30m: $\lambda/D \sim 1.5mm/30m \sim 10$ arcsec.

- Confusion

   Large antennas with enough sensitivity to detect

   more than one source within the beam are confusion limited.

- Small scale structure in radio sources

   galactic nuclei, hot spots in radio galaxies $\sim$ 0.1 - 1 arcsec

   molecular jets, filaments in crab nebula $\sim$ 1 arcsec

   IR sources, OH and masers in star formation regions $\sim$ 1 - 10 arcsec

   molecular cloud structure $\sim$ 0.1 arcsec - several degrees

   spiral arm structure in galaxies $\sim$ 1 arcsec - a few degrees

   quasars: VLBI $\lambda/D \sim 3$ mm/3000 km $\sim$ 0.2 milliarcsec.

- Spatial Dynamic Range to observe structures over a wide range of angular scales.

   single antennas can image structures larger than $\sim 20''$ at 3mm.

   need effective antenna diameters $\sim$ 1 kilometer to image arcsec structures.

- Techniques for high resolution observations

  lunar occultation

  interplanetary scintillation

  interferometers and aperture synthesis

2 APERTURE SYNTHESIS

2.1 Radio Antennas: Area, Resolution, Confusion, Cost

- Collecting area and point source sensitivity $\sim \eta N D^2$

- Mosaicing and extended source sensitivity $\sim \eta N D$

- Field of view of antennas $\sim \lambda/D_{ant}$.

- Spatial Dynamic Range $\sim \lambda/D_{min} - \lambda/D_{max}$

- Antenna cost $\sim N D^2 \lambda^{-0.7}$, where λ is $20 \times$ RMS surface accuracy.

2.2 Aperture Arrays

- Single dishes may have enough collecting area, but need more angular resolution.

- Antenna Arrays separate the functions of resolution and collecting area.

- Antenna Arrays sample the wavefront across a distributed aperture
    we measure the coherence of the wavefront across the array of antennas.
    electronics and signal transmission from the antenna need to preserve phase.
    atmospheric attenuation and path length fluctuations distort the wavefront.
    we must compensate for these effects. This is quite difficult.

- The problem is rather like adaptive optics.
    we must keep the path lengths within $\sim \lambda/20$ to make an accurate telescope.
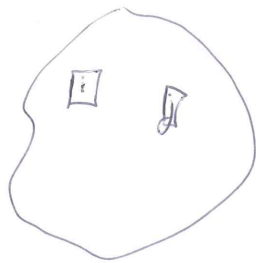
$$\left(\sum E_i \, \cos(\omega t + \phi_i) \right)^2$$

$$\sum E_i^2 \; + \; \sum_{i \neq j} E_i E_j \, \cos(\phi_i - \phi_j)$$

Total power.   cross product   relative phase.

Unfilled apertures

$+$, T's and circles
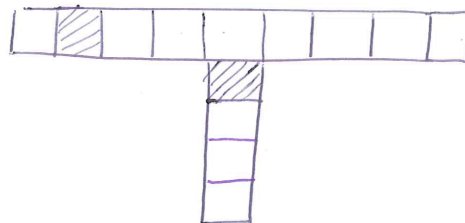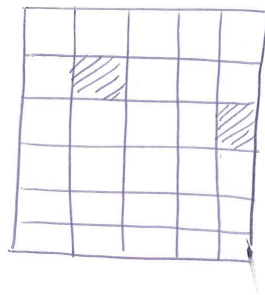
weighting different ⟶ synthesised beam.

2.3   Aperture Synthesis

• Consider aperture as set of antennas each with its own E-field and phase.

$$\text{Voltage response} = \Sigma \; E_i \; cos(\omega \; t + \phi_i)$$

$$\text{Power} = (\Sigma \; E_i \; cos(\omega \; t + \phi_i))^2 = \Sigma \; E_i^2 + \Sigma \; E_i \; E_j \; cos(\phi_i - \phi_j)$$

   sum of total powers from all antennas + cross products of all antenna pairs

   cross correlations contain information about wavefront across the aperture.

• Sample different pieces of the aperture at different times.

   we must preserve relative phase across the whole aperture to synthesize a large telescope.

• Skeleton arrays

   T-arrays contain same relative spacings as square apertures, but weighting is different.

   T-array has a different shaped beam because of different weights for each cross product, $E_i \; E_j$

2.4   Interferometer Arrays

- Response of a 2-element interferometer to point source:

$$P(s) = V_i(s) \ V_j^{\star}(s) \ \exp \frac{2\pi i}{\lambda} \mathbf{b}.\mathbf{s_0}$$

  $\mathbf{b}$ is the vector separation of the antenna pair (i, j), $\mathbf{s_0}$ is a unit vector in the direction of the source.

- $\mathbf{b} = (\mathbf{b_N}, \mathbf{b_E}, \mathbf{b_Z}) = (\mathbf{b_x}, \mathbf{b_y}, \mathbf{b_z}) = (\mathbf{u}, \mathbf{v}, \mathbf{w})$

  topocentric coordinates.

$$b_N = -b_x * sinl + b_z * cosl$$
$$b_E = b_y$$
$$b_Z = b_x * cosl + b_z * sinl$$

- $\mathbf{s_0} = (\mathbf{HA}, \mathbf{DEC}), (\mathbf{AZ}, \mathbf{EL}), (\mathbf{X}, \mathbf{Y}, \mathbf{Z})$

- (u,v,w)

$$u = b_x \ sin \ h + b_y \ cos \ h$$
$$v = (-b_x \ cos \ h + b_y \ sin \ h) \ sin \ \delta + b_z \ cos \ \delta$$
$$w = (b_x \ cos \ h - b_y \ sin \ h) \ cos \ \delta + b_z \ sin \ \delta$$

2 - element Interferometer

$V_1 \sim E\, e^{j\omega t}$

$V_2 \sim E\, e^{j(\omega t - \phi)}$ $\underline{S}$

$\underline{\underline{B}}$
⊗

$R \sim E^2 \exp\left[\dfrac{2\pi}{\lambda} j\, \underline{B} \cdot \underline{S}\right]$

$B \cdot S$

$\underline{S}$

$\underline{B}$

Earth Rotation Aperture synthesis

$\underline{S}$

$\underline{\underline{B}}$
(A) — (B)

δ

H
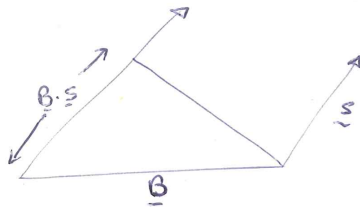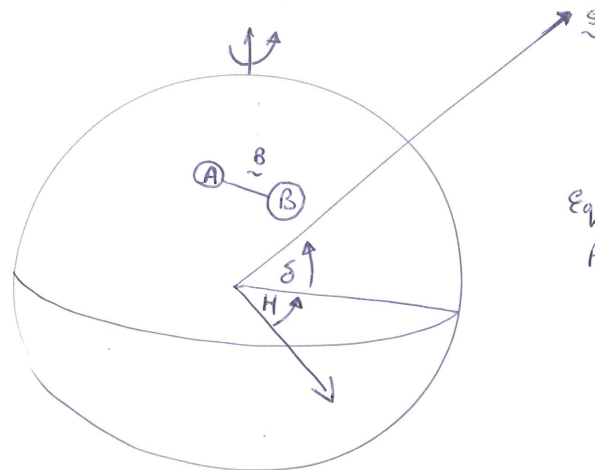
Equatorial coordinates (α, δ)

Astrometric coordinates (u, v)

29

2.5 Earth Rotation Aperture Synthesis.

- Interferometer array of small antennas tracking a target across the sky
  samples the aperture plane due to the Earth's rotation.

- Each antenna pair sweeps out a trajectory in the aperture plane.

$$V(t) = \int I(s)A(s - s') \exp \frac{2\pi i}{\lambda} \mathbf{b.s} \, ds$$

s' is pointing center
s_0 is phase tracking center
$\sigma = s - s_0$ is the vector from the phase tracking center to the source

$$V = \exp \frac{2\pi i}{\lambda} \mathbf{b.s_0}(t) \int I(\sigma)A(s - s') \exp \frac{2\pi i}{\lambda} \mathbf{b.\sigma} d\sigma$$

$$\text{Instrumental terms} \qquad \text{Source structure}$$

$\sigma = (x, y, z); \; b = (u, v, w)$

- If σ is small, then we can neglect curvature of the sky and write this as a 2D Fourier transform.

$$V(u, v) = \int I(x, y)A(x - x', y - y') \exp \frac{2\pi i}{\lambda}(ux + vy) \, dxdy$$

- 3D transform, "w projection", or faceting is needed to image large sources.

- An interferometer array is a chromatic instrument,
  we must use a small range of λ or else we get bandwidth smearing.
  for wideband continuum sources, we can use multi frequency synthesis, MFS,
  to obtain more Fourier samples of the brightness distribution.

2.6   Imaging

- We only have discrete samples of V, so we define a weighting function W, and evaluate:

$$I'(x,y) = \int W(u,v)V(u,v)\exp\frac{-2\pi i}{\lambda}(ux+vy)\,dudv$$

- The weighting function W can have any value where V is sampled

    $W = 0$ where V is not sampled.

- I' is The Fourier transform of the product of V and W,

    which is the convolution of the Fourier transforms of V and W:

$$I'(x,y) = B(x,y) \star [I(x,y)A(x,y)]$$

  where

$$B(x,y) = \int W(u,v)\exp\frac{-2\pi i}{\lambda}(ux+vy)\,dudv$$

  B is the synthesized beam.

- For a point source of unit amplitude at the phase tracking center, V(u,v)=(1,0).

    the synthesized beam is the interferometer point source response,

    analogous to the point-spread function in an optical telescope.

- Choice of natural, uniform, robust weighting: effect on the synthesized beam

2.7 Array Configurations

- Sample the wavefront in the aperture ; the (u,v) plane

- Minimum Redundancy Arrays.

  Linear arrays with few repeated spacings (Alan Moffet, 1968, IEEE AP-16, 172.):

  .1.2.   .1.3.2.   .1.3.2.2.1.   .1.3.3.2.   .1.5.3.2.2.

- East-West Minimum Redundancy Arrays and Synthesized Beams.

- (u,v,w)

$$u = b_y \ cos \ h$$
$$v = b_y \ sin \ h \ sin \ \delta$$
$$w = -b_y \ sin \ h \ cos \ \delta$$

- Two dimensional Array Configurations and Synthesized Beams.

$$u = b_x \ sin \ h + b_y \ cos \ h$$
$$v = (-b_x \ cos \ h + b_y \ sin \ h) \ sin \ \delta + b_z \ cos \ \delta$$
$$w = (b_x \ cos \ h - b_y \ sin \ h) \ cos \ \delta + b_z \ sin \ \delta$$
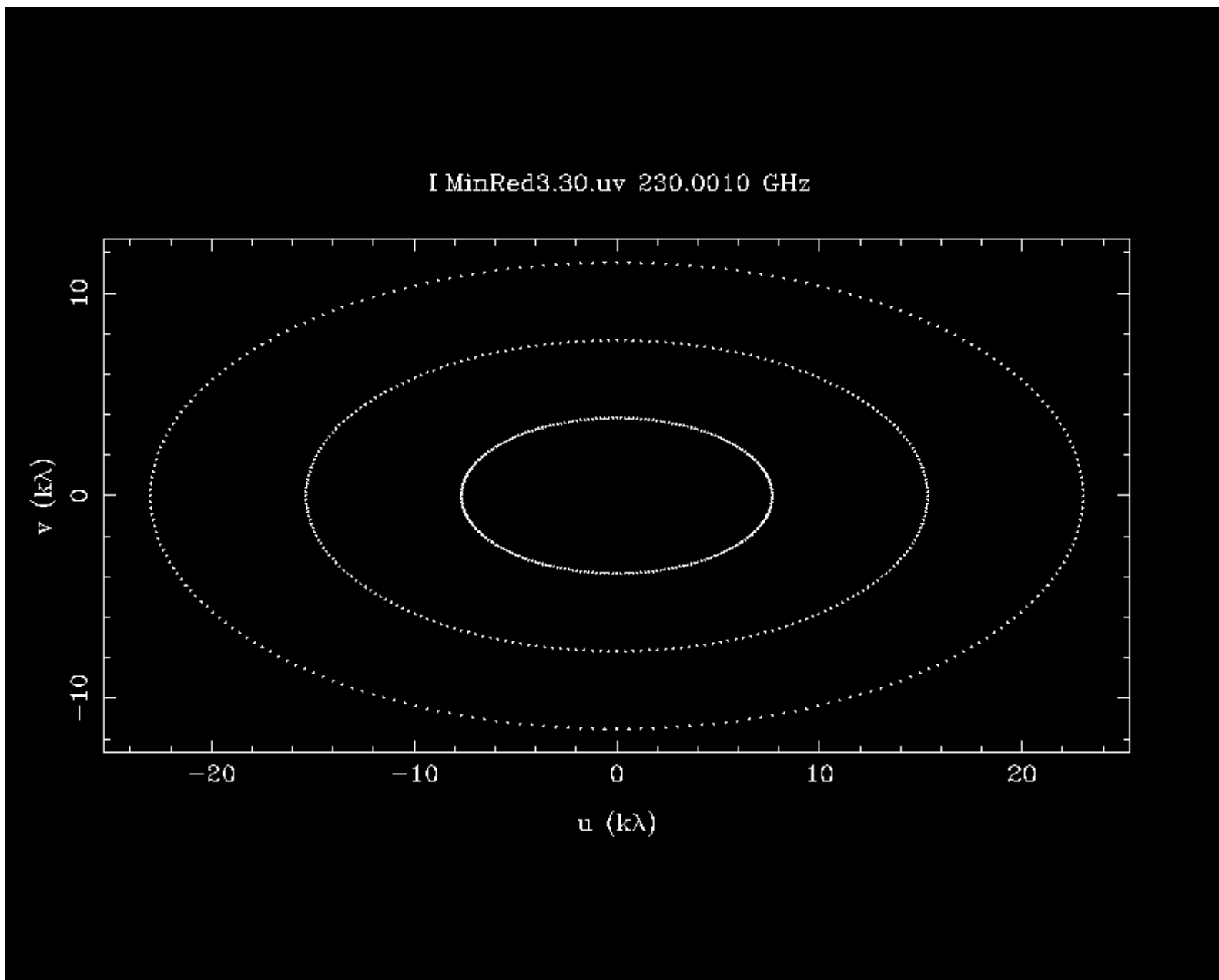
Figure 6: Aperture Synthesis: Minimum Redundancy Arrays: 3-antenna east-west array with 3 spacings. DEC=+30 degrees. HA= -6 to 6 hr. (Alan Moffet, 1968, IEEE AP-16, 172.). $MIR/demo/carma/mfs.csh MinRed3 30 -6,6,.1 1 sup=0 '-shadow(6.1)'

33

MinRed3.3

23:23:25.803   30:00:00.000

File: MinRed3.30.bm
Restfreq:230.000000 (GHz)
Crval3:   230.0010 GHz
Max: 1.00000
Min: −0.237874
Units: JY/BEAM

Axes: 256 x 256 x   1
      −2.24 x   4.48 x   0.50

Contours: 20

0.050	0.100
0.150	0.200
0.250	0.300
0.350	0.400
0.450	0.500
0.550	0.600
0.650	0.700
0.750	0.800
0.850	0.900
0.950	1.000

230

Relative DEC (″)

100   50   0   −50   −100

50   0   −50

Relative RA (″)
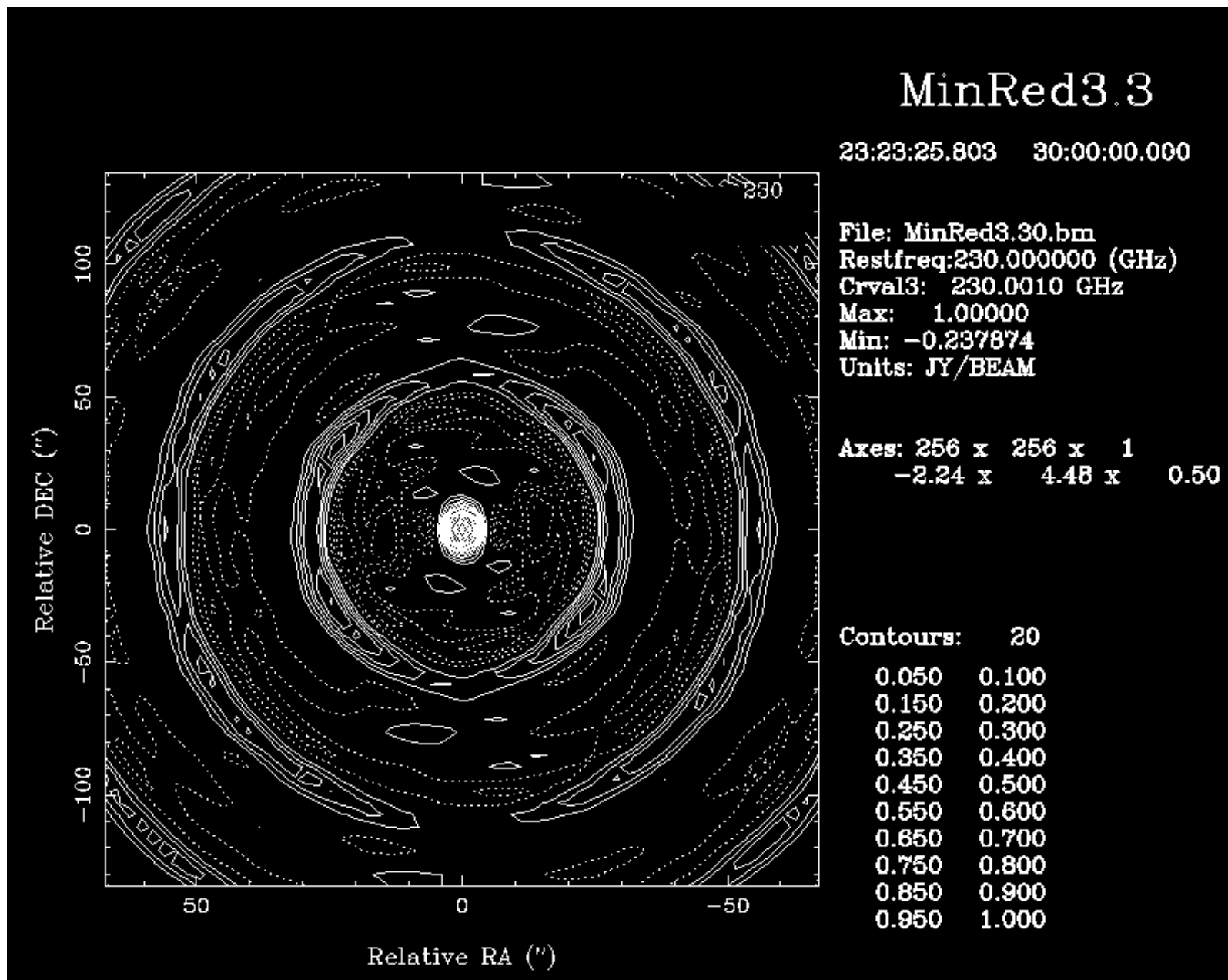
Figure 7:   Synthesized beam for 3-antenna east-west array with 3 spacings. DEC=+30 degrees. HA= -6 to 6 hr. $MIR/demo/carma/mfs.csh MinRed3 30 -6,6,.1 1 sup=0 '-shadow(6.1)'
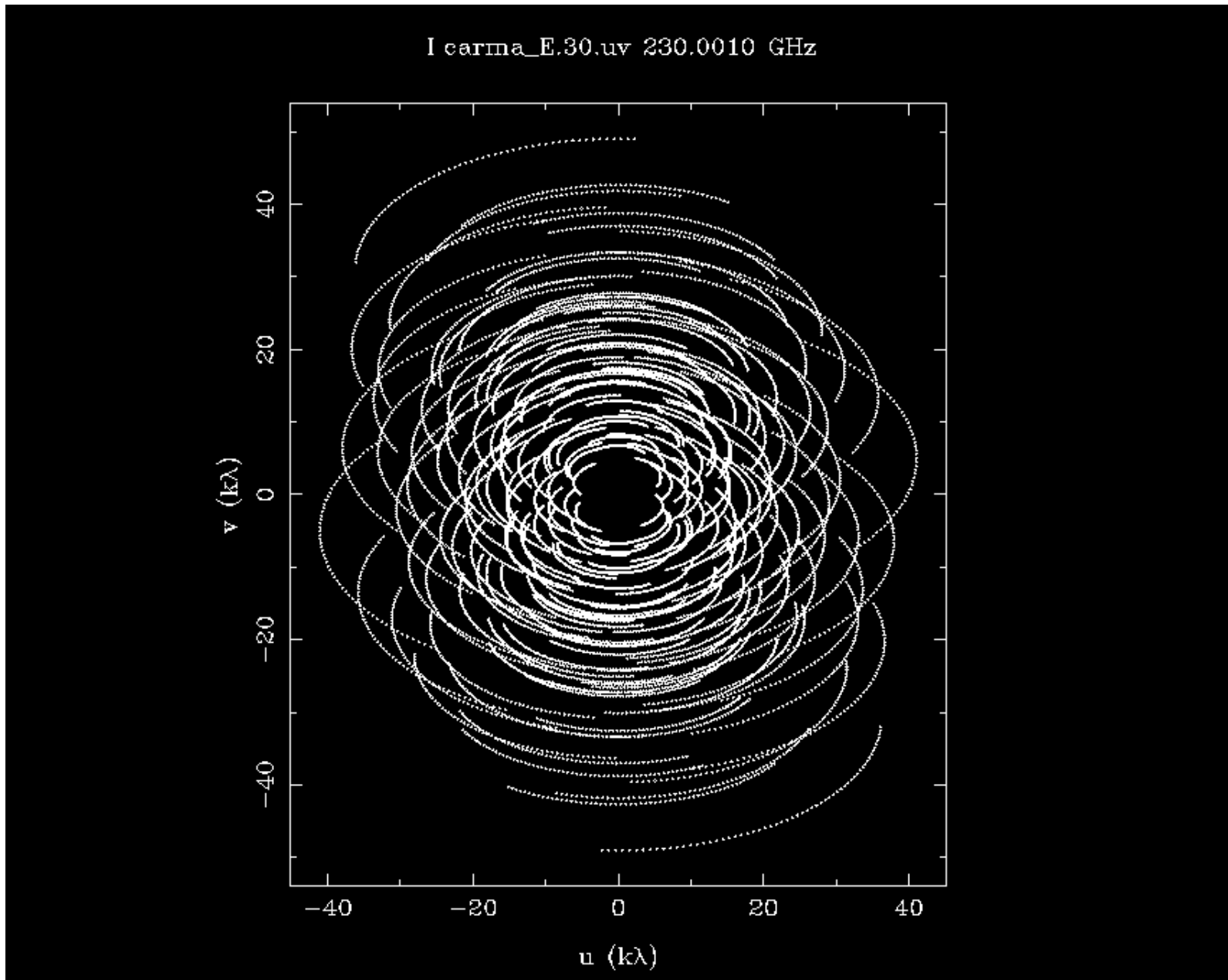
Figure 8:   CARMA 15-antenna E -configuration at DEC=+30 HA= -3 to +3 hr.
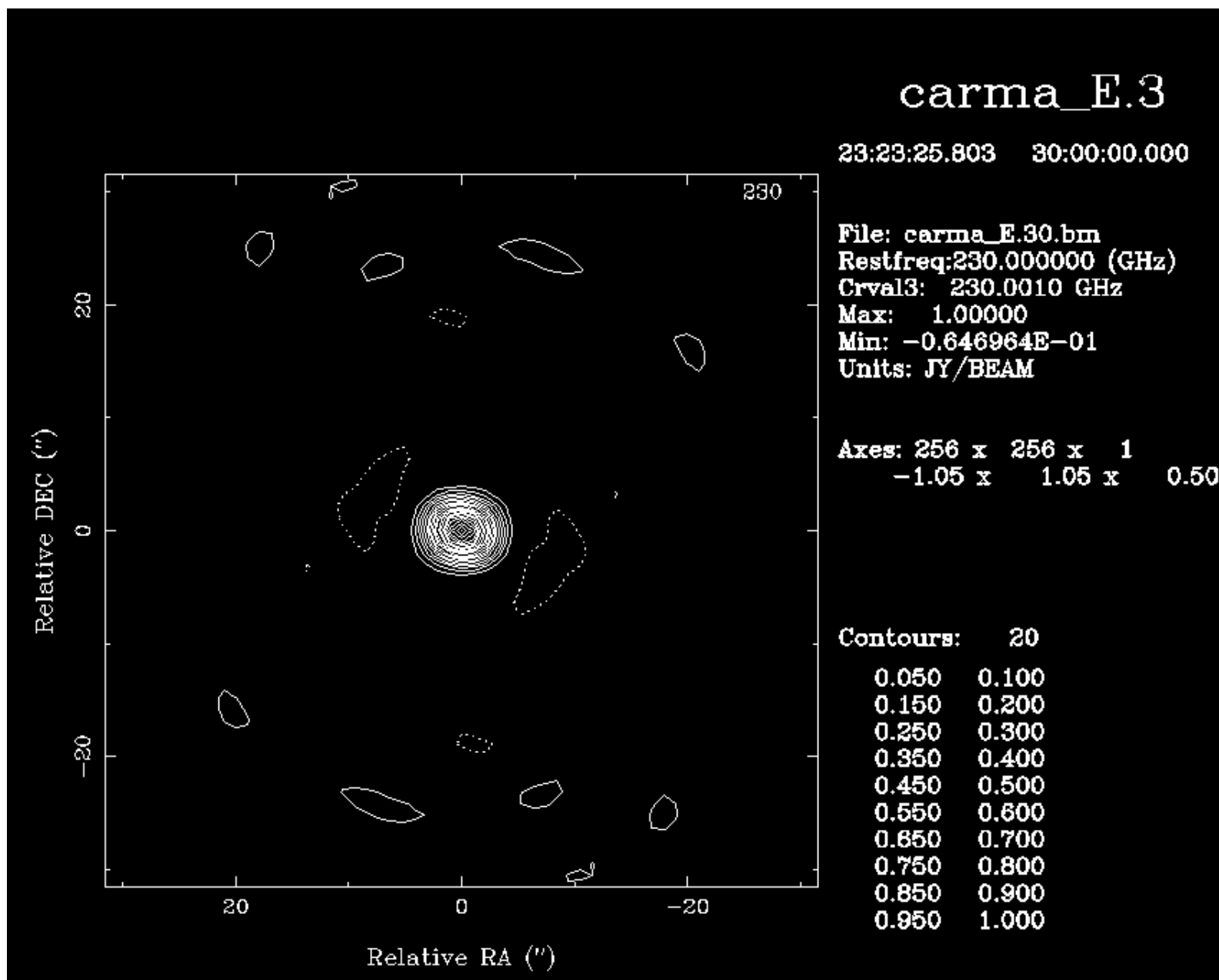
Figure 9:   Synthesized beam for carma E configuration at DEC=30, with HA -3 to 3 hr.

```
          ---   CARMA Single Field MFS Imaging     ---
     config    =   carma_D
     dec       =   30
     harange   =   -1,1,.1  hours
     nchan     =   1
     select    =   -shadow(10.4)
     freq      =   230
     imsize    =   256
     systemp   =   80,290,0.26
     jyperk    =   73
     bandwidth =   500


        ---   RESULTS    ---
     UVGEN:        2100 records written to file: carma_D.30.uv
```

Config	DEC	HA	Rms	Beam	Tb_rms	Sidelobe[%]			Nvis	uvrange[m]		weighting
Config	deg	hrs	mJy	arcsec	mK	Rms	Max	Min	%	min	max	
carma_D	30	-1,1	0.72	2.18 x 1.90	4.0	2.7	14.9	-6.8	100	10.5	147.3	sup=0
carma_D	30	-1,1	0.75	1.98 x 1.62	5.4	2.4	12.9	-11.5	100	10.5	147.3	robust=0.5
carma_D	30	-1,1	0.85	1.88 x 1.42	7.4	2.5	12.7	-14.4	100	10.5	147.3	uniform
carma_D	-30	-1,1	2.15	4.12 x 1.95	6.2	2.8	15.7	-9.1	60	6.3	103.5	sup=0
carma_D	-30	-1,1	2.23	3.63 x 1.80	7.9	2.5	15.4	-13.9	60	6.3	103.5	robust=0.5
carma_D	-30	-1,1	2.41	3.30 x 1.72	9.8	2.5	16.2	-18.4	60	6.3	103.5	uniform
carma_E	30	-1,1	0.72	4.40 x 3.92	1.0	2.6	14.2	-7.0	100	2100	8.1 66.3	sup=0
carma_E	-30	-1,1	2.45	7.72 x 3.28	2.2	2.4	18.5	-15.6	53	1122	3.3 54	uniform
carma_E	30	-1,1	0.72	4.40 x 3.92	1.0	2.6	14.2	-7.0	100	2100	8.1 66.3	sup=0
carma_E	30	-1,1	0.84	3.77 x 3.03	1.7	2.4	12.9	-15.3	100	2100	8.1 66.3	uniform

2.8   Properties of Synthesized Beam

– Resolution $\sim \lambda/2D_{max}$, where D_{max} is the maximum antenna separation.
note factor of 2 since $V(-u) = V^{\star}(u)$, the width of the aperture is $2D_{max}$.

– Aliasing of structures $> \lambda/D_{inc}$, where D_{inc} is the sample interval in the (u, v) data.

– Shortest spacing problem
source is "resolved" if size $>\sim \lambda/2D_{min}$, where D_{min} is the shortest antenna separation.

– Shortest spacing $>$ dish diameter D_{ant}, else collision or shadowing.

– Field of view of antennas $\sim \lambda/D_{ant}$.

– Each antenna configuration is sensitive to a range of angular sizes, $\lambda/D_{max}\ -\ \lambda/D_{min}$

– We must select sources with structures between $\lambda/2D_{ant}$ and $\lambda/2D_{max}$ in order to image with a single pointing.

– Larger structures can be imaged using multiple pointing centers in a mosaic.

CARMA Synthesized beams and antenna spacings at 230 GHz.

	$D_{min}[m]$	$D_{max}[m]$	*Synthesized beam*["]	λ/D_{min}["]
a-array	142	1884	0.13x0.11	2.8
b-array	82	946	0.33x0.26	4.7
c-array	25	373	0.8x0.6	15.6
d-array	10.2	148	1.7x1.4	39.
e-array	7.5	66	3.5x2.8	52.

/siomaps/fig32.wip

sioABC5.cm

sioA5.cm
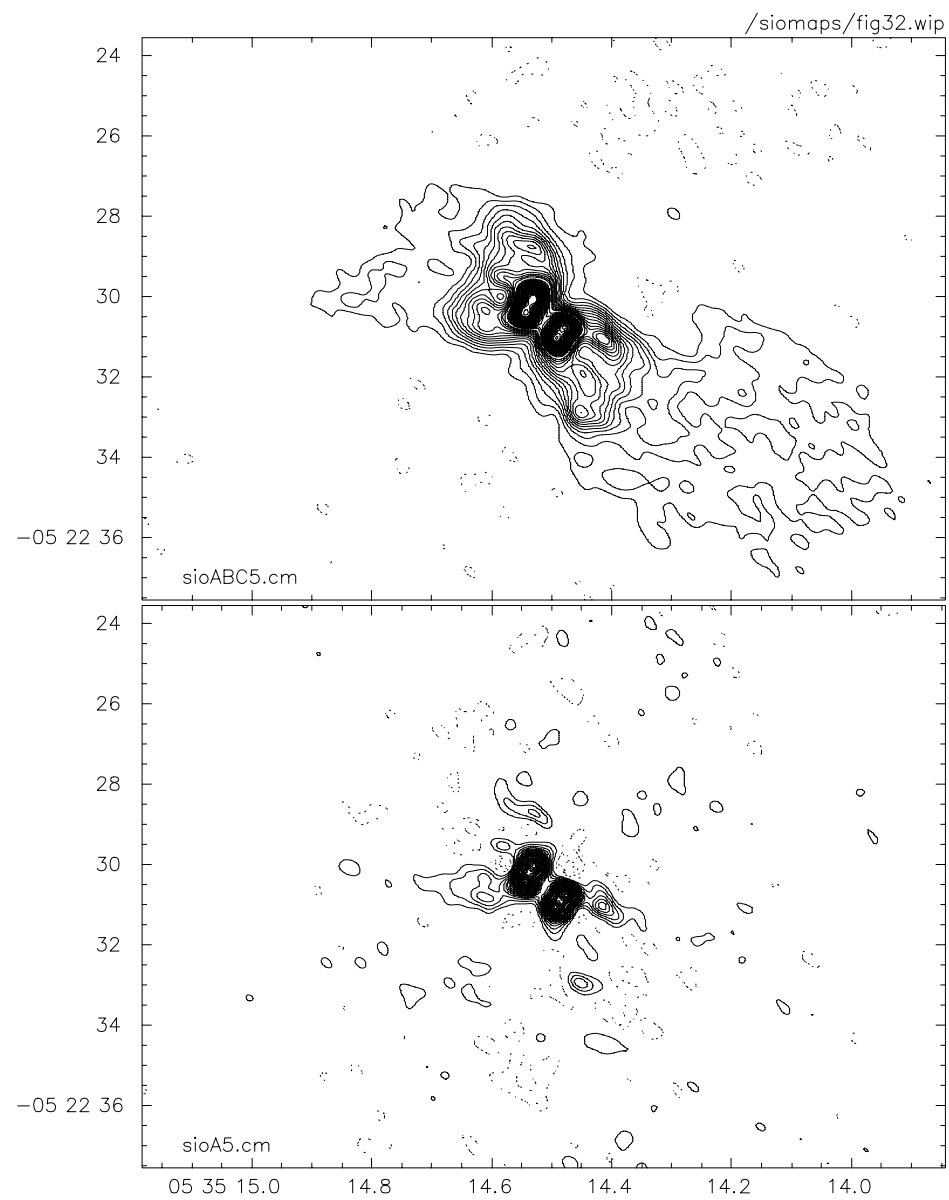
2.9 Primary Beams

– Interferometer Primary beam pattern illuminates the Field of view.

– Primary beam for an interferometer is the cross power pattern.
  for each antenna pair (i, j),
$$A_{i,j}(\mathbf{s}) = V_i(\mathbf{s}) \times V_j^\star(\mathbf{s})$$

– Illumination, or weighting of the FOV may be different for each antenna pair (i, j)

– Within 5% level, primary beam patterns are Gaussian.

CARMA Primary Beams at 230 GHz

Antennas	Equivalent diameter	FWHM	Nyquist interval
m x m	m	arcsec	arcsec
10.4 x 10.4	10.4	28	12.5
10.4 x 6.1	8.0	36	
6.1 x 6.1	6.1	47	21.3
10.4 x 3.5	6.0	48	
6.1 x 3.5	4.6	63	
3.5 x 3.5	3.5	83	37.1

2.10   Deconvolution

- Deconvolve the synthesized beam response from the image I'.

$$I'(x, y) = B(x, y) \star [I(x, y)A(x, y)] + Noise$$

  Two different algorithms:

  CLEAN - iterative point source subtraction algorithm

  MAXIMUM ENTROPY - maximum likelihood image consistent with the data.

- Image Model, $M(x, y)$, after deconvolution

  $I' = B(x, y) \star M(x, y) + Resid(x, y)$

  $M(x, y)$ is an estimate of $I(x, y)A(x, y)$

- RESTOR - convolve Model by Gaussian with same FWHM as synthesized beam

  $I_1(x, y) = G(x, y) \star M(x, y) + Resid(x, y)$ the default "clean" image

  $Resid(x, y) = I'(x, y) - B(x, y) \star M(x, y)$ mode=residual

  $I_2(x, y) = G(x, y) \star M(x, y)$ mode=convolve

3   OBSERVING PREPARATION

3.1   Overview of Observation Preparation

- Select Science target source(s)

  Science requirements: Resolution, Spatial dynamic range, Field of view, Sensitivity

  $$Source\ size < Primary\ beam\ FWHM?$$

  True: Single pointing.
  False: Multiple pointings needed. Determine number of mosaic pointings.

  $$\lambda/D_{max} > Source\ size > \lambda/D_{min}?$$

  True: Estimate image size and calculate brightness sensitivity in synthesized beam.
  False: Not a good match to this antenna configuration.

- Select Observing frequency(s)

  Spectral line – select correlator configuration.

  Continuum – maximum bandwidth. Calculate sensitivity.

- Select Calibration sources

  – close to target source.

  – strong enough to get a good calibration.

  – bandpass calibration.

  – absolute flux calibration.

  – atmospheric phase calibration.

- Prepare Observing Script.

3.2 Science Targets

- what are the Science Goals ?

- what are the instrumental requirements to meet these goals ?

- is this project a good match to CARMA capabilities ?

- Field of view - angular size of source region ?

  single pointing center or mosaic observation.

  if multiple pointings needed are these contiguous ?

- Angular resolution required ?

  sufficient resolution to see the structures of interest.

- Sensitivity

  what is the expected brightness of the source ?

- Spatial dynamic range.

  what is the range of angular scales we need to measure ?

  each antenna configuration is sensitive to a range of angular sizes, $\lambda/D_{max} - \lambda/D_{min}$

3.3   Observing Frequency

- Spectral line observations ?

  select correlator configuration.

  calculate sensitivity at the velocity resolution needed.

- Continuum observation.

  maximum bandwidth currently eight 500 MHz bands = 16 x 500 MHz windows.

  calculate sensitivity.

- 3mm or 1mm observations ?

  what spectral lines are best ?

  what is the spectral index of the continuum emission ?

  calculate sensitivity.

3.4 Calibration

- Observe calibration sources to estimate $G(t, f, p)$

$$V' = G \times V + thermal\ noise$$

  V is the true source visibility and G is the calibration factor.

- Gain calibration (amplitude and phase versus time)

  observe a strong point source at 20 - 30 min intervals.

- Bandpass calibration.

  usually a strong compact source

- Absolute flux calibration.

  usually a planet whose flux can be calculated.

- Calibration Errors

  for each calibration, the error in the measured visibility is given by:

$$\delta V' = \delta G \times V + thermal\ noise$$

  calibrator must be strong enough to get a good calibration.

  calibrations are themselves limited by thermal noise.

  balance between time calibrating and time on target.

  random thermal noise is better than systemic calibration errors.

  strong sources: we need to work harder on calibration.

  weak sources: better to spend more time integrating on the target source.

3.5 CARMA Telescope Characteristics.

- CARMA is a heterogeneous array with six 10.4m and nine 6.1m antennas.

- Five array configurations giving resolution $\sim 0.1, 0.3, 0.7, 1.8, 3.2''$ at 230 GHz.

3.6 Primary beam and Synthesized beam

- Primary beamwidth, $FWHM \sim 1.2 \; \lambda/D_{ant}$

- Synthesized beamwidth, $FWHM \sim \; \lambda/D_{max}$

- Primary beam illuminates the sky brightness distribution.
  — sources smaller than primary beam can be observed with a single pointing
  — sources larger than the primary beams need multiple pointings
  — we MUST allow for the different primary beam patterns of 10 and 6m antennas.

- Spatial Dynamic Range
  — each antenna configuration is sensitive to a range of angular sizes, $\lambda/D_{max} \; - \; \lambda/D_{min}$
  — source structure larger than λ/D_{min} is "resolved out" by the interferometer.
  — source structure larger than λ/D_{min} needs complementary single dish observations.

3.7 Mosaicing

- Sources larger than the primary beam need multiple pointings

  to image large scale structure needs overlapping pointings.

  Nyquist sample interval $\lambda/2D_{ant}$ – see Table.

  use same pointing centers for 10 and 6m antennas.

- Within 5% level, primary beam patterns are Gaussian.

CARMA Primary Beams at 230 GHz

Antennas	Equivalent diameter	FWHM	Nyquist interval
m x m	m	arcsec	arcsec
10.4 x 10.4	10.4	28	12.5
10.4 x 6.1	8.0	36	
6.1 x 6.1	6.1	47	21.3
10.4 x 3.5	6.0	48	
6.1 x 3.5	4.6	63	
3.5 x 3.5	3.5	83	37.1

3.8 Sensitivity

- System Temperature

  $T_{sys} = \left[T_{sky} \ (1 - e^{-\tau}) + T_{source} + T_{ant} + T_{Rx} \right] \times \ 2 \ e^{\tau}$

  (single sideband observations with double sideband receivers)

  noise fluctuations $\Delta T = T_{sys}/\sqrt{2 \ Bt}$

  B is the bandwidth, and τ is the atmospheric opacity.

  total integration time, $t = $ N(N-1)/2 x time on source.

- Antenna Temperature

$$k \ T_a = 0.5 \ S \ \eta \ A$$

- Aperture efficiency = illumination efficiency x surface efficiency

$$JyperK = Jansky/Kelvin = S/T_a = (2k/\eta A)$$

CARMA Aperture Efficiency

antenna	$2k/A$	$\eta = 0.7$	$\eta = 0.5$
10.4 m	32	46	65
6.1 m	94	135	189

3.9   Flux and Brightness Sensitivity

• Flux sensitivity

$$\Delta S = \Delta T \times Jy/K = \Delta T \ (2k/\eta A)$$

• Brightness Sensitivity

flux density, S within the synthesized beam correspond to brightness temperature, T_b.

$$\Delta S = 2k \ \Delta T_b/\lambda^2 \times \delta \Omega$$

for a Gaussian synthesized beam $\delta \Omega = \pi \ \theta_x \ \theta_y/4log2$

• Examples:

1. Continuum observations, BW=1500 MHz, DEC=30 degrees, time on source $\sim$ 5 hr

2. Line observations, line width = 10 km/s, DEC=30 degrees, time on source $\sim$ 5 hr

CARMA Sensitivity in $\sim$ 5 hr

GHz	Tsys	BW	η	Ω	ΔS	ΔT_b
100	200	1500 MHz	0.7	$5.5 \times 4.5''$	0.4 mJy	1.9 mK
115	400	1500 MHz	0.7	$4.8 \times 3.9''$	0.7 mJy	3.6 mK
230	500	1500 MHz	0.5	$2.4 \times 2.0''$	0.9 mJy	4.5 mK
100	200	10 km/s	0.7	$5.5 \times 4.5''$	8 mJy	40 mK
115	400	10 km/s	0.7	$4.8 \times 3.9''$	15 mJy	72 mK
230	500	10 km/s	0.5	$2.4 \times 2.0''$	13 mJy	63 mK

************ DEMO THE CARMA RMS CALCULATOR ************

http://cedarflat.mmarray.org/observing/tools/rms.html

4 OBSERVING PROCEDURES

4.1 Observing scripts

- Select suitable observations for the target sources.
    - sensitivity
    - source size; mosaicing.

- CARMA correlator capabilities; select correlator settup.

- Choose calibrators for gain, bandpass, flux and pointing.

4.2 Summer School Observing Projects

- Group discussion selecting student projects.

- More students this year – 2-3 students for each project.

- After discussion period, each group should
    - email one paragraph about project to memo organizer (Marc)
    - insert project via proposal web page

4.3 Observer's everyday responsibilities

• creating and running the master schedule

• decide whether to do 1 mm or 3 mm

• data quality reports

• flux calibration/array health tasks

• first line of troubleshooting

4.4 Troubleshooting

• generator, air conditioning

• anticollision system

• cryogenics

• rcvr tuning

• computer hangups

• clocks; resetting the time
  - rebooting procedure

4.5   Calibrating a new array configuration

- change IFLO connections in the pits

- run tilt, shimming the antennas

- enter new station coordinates

- find pointing offsets.

- find the delay centers

- TV and radio pointing

- find a baseline

- enter new pointing offsets and antenna positions.

5 DATA INSPECTION AND EDITING

5.1 Introduction to MIRIAD

- **M**ultichannel **I**mage **R**econstruction, **I**mage **A**nalysis and **D**isplay.

  tasks controled by keywords operate on the data.

- Miriad uvdata format

  "stream" of data and metadata stored as "items" in datasets.

  e.g. **ct007.1C.3C273.miriad/**

  bandpass flags gains header history leakage vartable visdata

- uvdata structure

  multiple sources, frequencies, mosaics, polarization, interferometer or single dish

  visdata stored as real, complex, or scaled 16-bit integers.

  vartable metadata are a stream of named variables and values.

  uvvariables source names, frequencies, pointing centers, can change in the data stream.

  history observation and data reduction, including command line parameters.

  flags binary flags for each frequency channel

  other items, e.g. WVR data, observing scripts and parameters, etc.

- calibration tables

  bandpass gains leakage

  calibration parameters are stored in the uvdata structure.

- Real-time Imaging.

  MIRIAD uvdata is well suited for real-time imaging.

  "stream" of data and metadata.

  data can be processed in close to real time.

  Aperture Synthesis Images at the telescope

- Image data.

  e.g. **3c273.mp**

  header history image mask

  same format for single field maps, beams, multichannel, MFS, mosaics, polarization,

  model images, clean, maxen, mfclean, mosmem, mossdi etc.

  header FITS-like format to describe multidimension image data.

  image stored as floating point numbers.

  mask bit-mask for pixel blanking.

  history observation and data reduction, including command line parameters.

5.2   MIRIAD documentation and help

• in-code documentation is extracted when code is complied.

• doc and mirhelp access documentation for tasks and source code.

   e.g. doc invert

   INVERT is a MIRIAD task which forms images from visibilities.

   e.g. -cN show recognized categories (N = 1, 2 or 3)

```
> doc -c1
General             Utility           Data Transfer     Visual Display
Calibration         uv Analysis       Map Making        Deconvolution
Plotting            Map Manipulation  Map Combination   Map Analysis
Profile Analysis    Model Fitting     Tools             Other
```

- List of routines by functional category

```
> doc -t $MIR/doc/prog/*.doc
```

```
*** 8. DECONVOLUTION ***
------------------------
clean      Apply Hogbom, Clark or Steer CLEAN algorithm to a map
maxen      Maximum Entropy deconvolution
mfclean    Multi-frequency synthesis CLEAN.
mfspin     Compute spectral index from a MFCLEAN model.
mosaic     Deconvolution using mosaicing method
mosmem     Maximum Entropy deconvolution for a mosaiced image
mossdi2    Mosaic Steer CLEAN algorithm
mossdi     Mosaic Steer CLEAN algorithm
mostess    Maximum Entropy deconvolution for a mosaiced observation
pmosmem    Maximum Entropy deconvolution for polarization mosaics
restor     Restore clean components to make the CLEAN map
tvcln      Clark/Steer CLEAN with display of intermediates
```

5.3   MIRIAD keywords

- Standard keyword: vis

    normal keyword for an input visibility dataset.

    there is generally no default input name.

    some tasks allow multiple input datasets with wildcards supported, such as an asterisk.

- Standard keyword: line

    the "line" parameter determines the channels that are to be processed from a uv data-set.....

- Standard keyword: select

    this keyword selects the subset of the visibility data to be processed.....

- Standard keyword: in

    name for an input dataset – usually an image....

- Standard keyword: region

    selects a subregion of an image.....

- Standard keyword: options

    this keyword is often used to specify extra processing options to a task......

5.4 Overview of data reduction procedure

- plot amplitude and phase vs. time (uvplt)
    - select the calibration sources

- plot amplitude and phase for the bandpass calibrator (uvspec)
    - look for bad data, phase coherence, jumps

- fit antenna based gains versus time and bandpass (mfcal, selfcal)

- plot gains and bandpass (gpplt)

- plot calibrated amplitude and phase for the calibration sources (uvplt)
    - calibrator amplitude should be S[Jy], and phase=0 (+ noise)

- image the calibrator (invert)

- deconvolve the synthesized beam (clean, restor, implot or cgdisp)
    - calibrator should be point source with peak S[Jy]

- image the target source(s) (invert options=mosaic line=...)
    - e.g. line= wide (continuum), or line=chan,nchan,start,width,step.

- autocal – tutorial script
    - csh script to calibrate MIRIAD uvdata using selfcal.
    - inputs specify the calibrator and line type to be used for calibration
    - inputs specify the source and line type to be imaged.

6   CALIBRATION

- Calibration of an interferometer array can be broken into 3 groups:

  1) component values, e.g. cable lengths, which change only when the system is re-built.

  2) array parameters which change after antenna moves.

  3) instrumental parameters which change with time or ambient conditions.

  (1) and (2) are handled by array staff and observers; (3) is responsibility of the user.

  (see BIMA memo 85)

6.1 Calibration Requirements

1) IF fiber and cable lengths, IF delay centers.

2) Power levels, correlation coefficient corrections.

3) Receiver and phase lock tuning parameters.

4) Pointing parameters, receiver feed (horn) offsets , TV camera offsets

5) Primary beam patterns, focus, subreflector position, Holography

6) Antenna positions, antenna geometry, array geometry.

7) System temperature, opacity, atmospheric model.

8) Flux density scale, antenna Jy/K.

9) Polarization, leakage corrections.

10) Bandpass, IF and RF frequency response.

11) Gains: amplitude and phase versus time; frequency switching.

12. Atmospheric decorrelation, fast switching, and water line radiometry.

13) Single dish

14) Editing, flagging and blanking.

15) VLBI, phased arrays.

6.2 Calibration corrections to interferometer equation

$$V(t) = G(t, f, p) \times \int I(s) A(s - s') \exp \frac{2\pi i}{\lambda} \mathbf{b}.\mathbf{s} \, ds$$

s' is pointing center
s_0 is phase tracking center
$\sigma = s - s_0$ is the vector from the phase tracking center to the source

$$V = G(t, f, p) \times \underbrace{\exp \frac{2\pi i}{\lambda} [\mathbf{b}.\mathbf{s_0}(t) - delay0]}_{\text{Instrumental terms}} \underbrace{\int I(\sigma) A(s - s' + \Delta s) \exp \frac{2\pi i}{\lambda} \mathbf{b}.\sigma d\sigma}_{\text{Source structure}} + offsets + noise$$

- $G(t, f, p)$ complex gain versus time, bandpass, flux density and polarization calibration.

- $delay0$ instumental and atmospheric delay calibration.

- $A(s - s' + \Delta s)$ pointing, focus and primary beam calibration.

- phase switch by π to cancel offset.

- phase switch by $\pi/2$ to separate USB and LSB of LO1.

6.3   Calibration Errors

- Observe calibration sources to estimate $G(t, f, p)$

    how strong and how close to target source ?

- Random noise

$$V' = G \times V + thermal\ noise$$

    V is the true source visibility and G is the calibration factor.

    for each calibration, the error in the measured visibility is given by:

$$\delta V' = \delta G \times V + thermal\ noise$$

- Systematic errors

    e.g. gain as a function of source or antenna position

6.4 Phase Calibration

- Time on calibrator

$$\delta S = (Jy/K) \times T_{sys}/\sqrt{(2Bt)}$$

for each baseline, $\delta S \sim 100 \times 150/\sqrt{(2 \times 10^9 \times 60)}, \sim 40mJy$

SNR ~ 25 on a 1 Jy source in 1 GHz BW in 1 minute, ~ 2 degrees of phase

antenna based calibration is better by $\sim \sqrt{(N_{ants} - 1)}$

- Angular separation between target source and calibrator

array geometry, thermal effects,...

slew time and suitable calibrator availability

- Phase calibration errors

we measure interferometer phase of target source w.r.t. calibrator

$$\phi = (2\pi/\lambda) \ \mathbf{b}.(s - s_{cal})$$

$$\delta\phi = (2\pi/\lambda) \ (\mathbf{b}.\delta s_{cal} + \delta\mathbf{b}.(s - s_{cal}))$$

e.g. $\delta\mathbf{b} \sim 0.1mm, \ \ \delta s_{cal} \sim 0.01'', \ \ \mathbf{b} \sim 2000m, \ \ (s - s_{cal}) \sim 50deg$

calibrator position error: $\mathbf{b}.\delta s_{cal} \sim 0.1mm$

antenna position error: $\delta\mathbf{b}.(s - s_{cal}) \sim 0.1mm$

- Observe gain calibrator as close to target as possible

prefer random thermal noise rather than systemic calibration errors.

6.5   Amplitude Calibration

- Primary calibration from planets

$$V'_{ij} = \int \frac{2k}{\lambda} T_b(s) A(s - s') \exp \frac{2\pi i}{\lambda} \mathbf{b.s} \, ds$$

  standard planet model uses $J_1(u, v)$ for uniform brightness disk

  selfcal uses uv-variables: **pltb plmaj plmin plangle**

- Secondary calibration from Quasars

  quasars are time variable, – sometimes very rapid.

  flux density history in **$MIRCAT/FluxSource.cat**

  interpolate calibrator flux to date of observation

```
e.g.
calflux source=3c273 in=$MIRCAT/FluxSource.cat device=/xs
```

6.6 Absolute gain calibration using planet observations

- absolute gain calibration using planet observations with a planet model in selfcal.

- if planet is resolved then gains depend on the detailed surface brightness distribution in planet model.

- for absolute flux calibration, correction must be made for absorption lines in planetary atmospheres.

IRR   223.0265 GHz

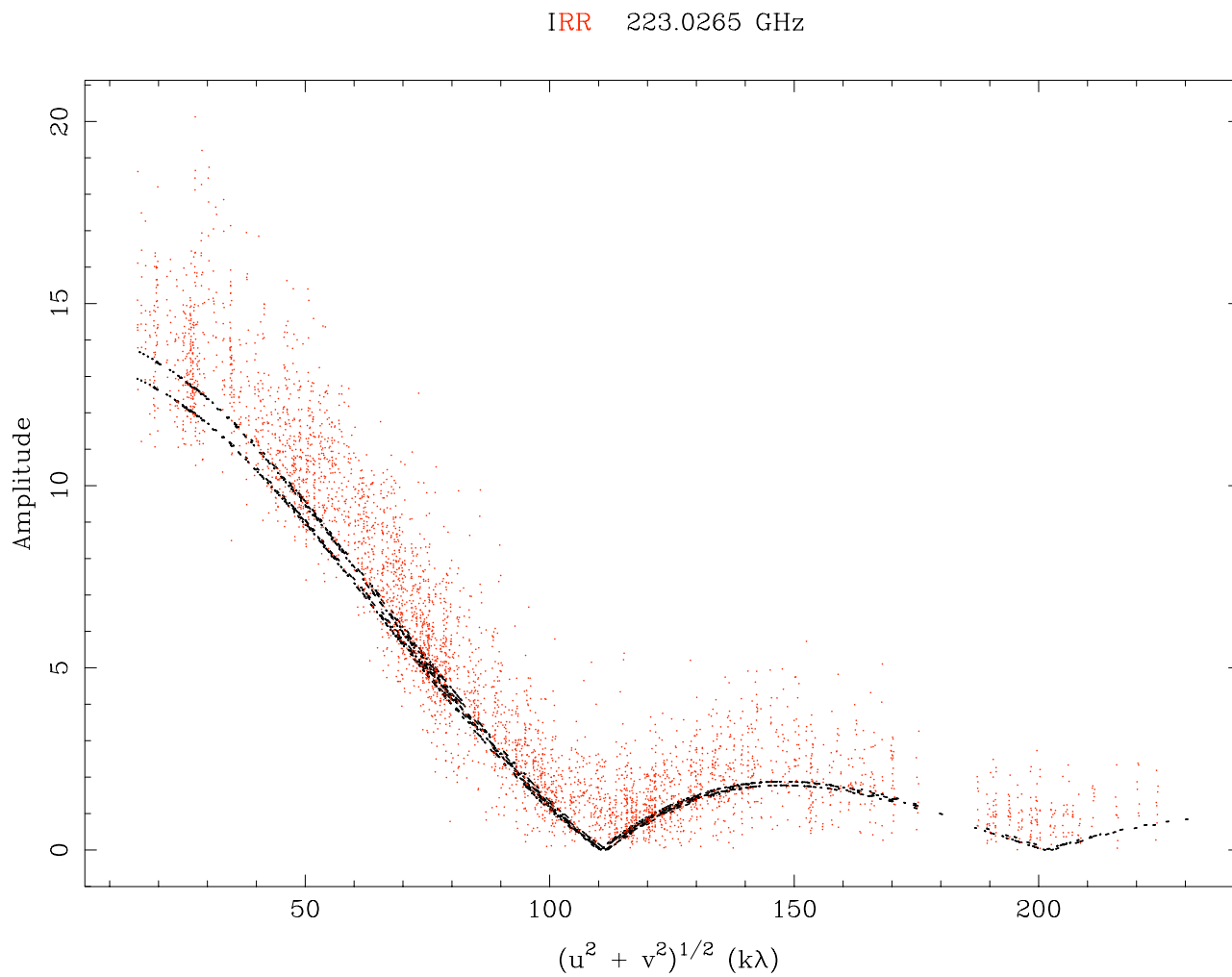Figure 11:   The solid lines show the model visibility for USB (229.65 GHz) and LSB (223.0 GHz), using a model uniform brightness disk with parameters: plangle: -23.7, plmaj: 2.29, plmin: 2.25, pltb: 97.5
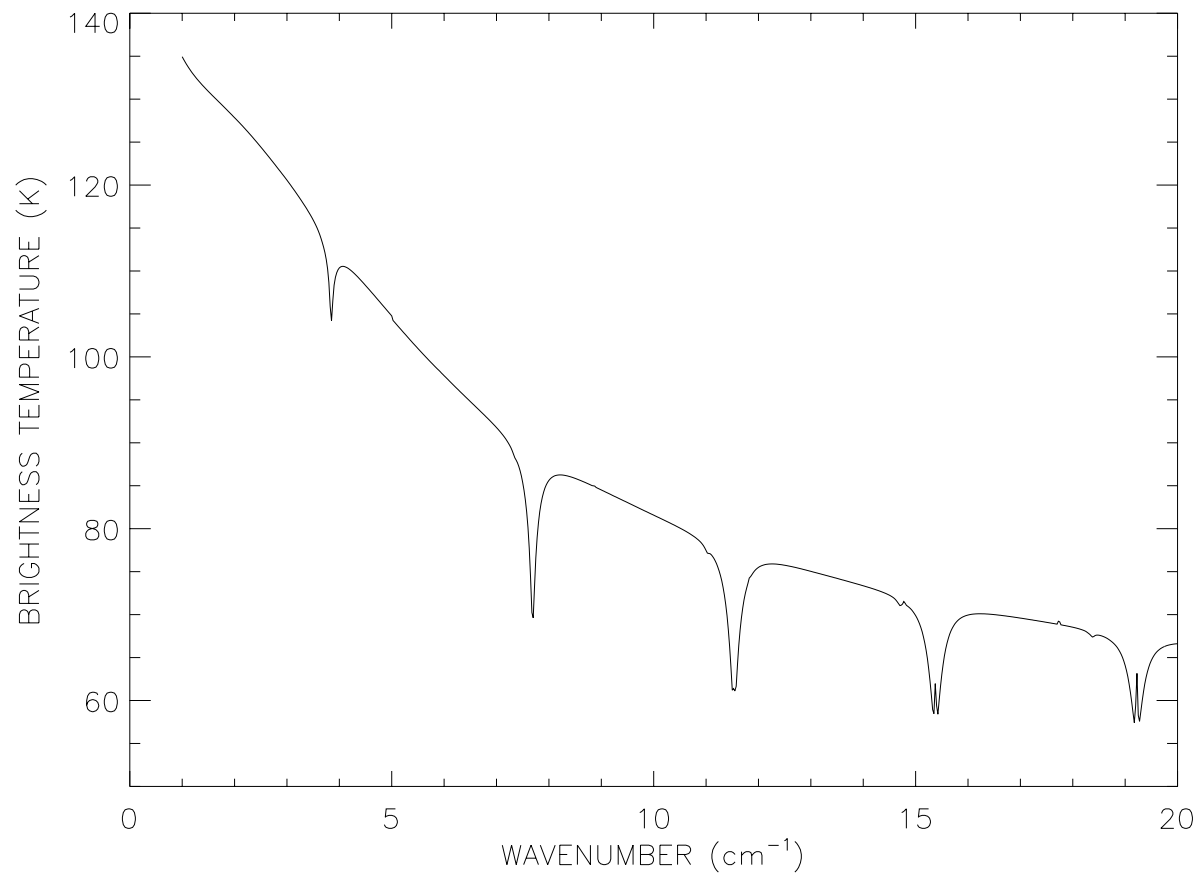
Figure 12: Brightness temperature of Neptune showing strong atmospheric absorption features. For absolute flux density calibration, correction must be made for absorption lines in planetary atmospheres.

6.7 Pointing Calibration

- Pointing model daz = daz(az,el); del = del(az,el)

    pointing model parameters describe:

    encoder offsets, antenna tilt, axis alignments, collimation errors, axis eccenticity

- Optical pointing on stars uses a small telescope with a CCD on each antenna.

- Radio pointing finds collimation errors w.r.t. optical pointing equations.

- After antenna move

    measure antenna tilt, and level using a tilt meter

    optical and radio pointing used to update the pointing model parameters.

- Pointing Errors

    Gaussian primary beam, $y = exp(-(\theta/\sigma)^2)$

    $\Delta y/y = -2\theta/\sigma^2 \times \Delta\theta$

    e.g. at FWHM $= 100''$, a $5''$ pointing error gives a 14% amplitude error.

6.8   Aperture Efficiency, Pointing and Primary Beam Calibration.

- traditionally separate calibrations, but better as integrated sequence

    aperture efficiency calibration needs good pointing

    primary beam calibration needs good pointing

- Hexagonal 7-pointing mosaic works very well (CARMA memo 52).

- Self-calibrated to determine the antenna voltage gains.

- Gaussian fits to the antenna voltage patterns

- Aperture efficiency:

    we measure 65 and 145 Jy/K;

    aperture efficiencies 50% and 65% for 10 and 6m antennas.

- Primary Beam at 100 GHz consistent with a common FWHM for azimuth and elevation.

    FWHM for 10m antennas is 1.20 +/- 0.02 arcmin.

    FWHM for 6m antennas is 1.98 +/- 0.03 arcmin.

- At 230 GHz, FWHM in elevation maybe slightly smaller ? (subreflector sag ?).

    FWHM azimuth: 0.55 +/- 0.02, elevation: 0.50 +/- 0.02 for 10m antennas

    FWMH azimuth: 0.86 +/- 0.02, elevation: 0.83 +/- 0.03 for 6m antennas.

6.9 Antenna Position Calibration

- calculated interferometer phase for calibrator

$$\phi = (2\pi/\lambda) \, \mathbf{b}.s_{cal}$$

- measured residual phase

$$\delta\phi = (2\pi/\lambda) \, (\mathbf{b}.\delta s_{cal} + \delta\mathbf{b}.s_{cal}) + noise$$

- for calibrator, $\delta s_{cal} \sim 0.01''$, $\mathbf{b} \sim 2000m$

    calibrator position error, $\mathbf{b}.\delta s_{cal} \sim 0.1mm$

- Observe quasars rapidly over a wide range of HA and DEC.

- Fit measured residual phase, $\delta\phi$ to solve for $\delta\mathbf{b}$.

6.10 Atmospheric phase calibration

- Atmospheric turbulence causes path length differences to each antenna.

  Kolmogorov spectrum, $\Delta path \sim baseline^{1/3}$ on long baselines.

  $\Delta path \sim 1mm$ at 1 km.

  mostly from water vapour fluctuations at mm wavelengths.

- Fast switching and Paired Antenna Calibration (PACS).

  reduce effective distance between source and calibrator

  $$d = \sqrt{([h(s - s')]^2 + [v \, \Delta t]^2)} \sim 140m$$

  height of atmospheric fluctuations (may be multiple layers), $h \sim 1$ km
  source-calibrator angle, $s - s'_i \sim 5\,\text{deg}$,
  turbulence speed, $v \sim 10$ km/s, and $\Delta t \sim 10$s.
  $h(s - s') \sim 100$m, and $v \, \Delta t \sim 100$m

  reduce atmospheric phase fluctuations on antenna baselines $>\sim 140$m

- Atmospheric phase coherence calibration.

  maybe needed if atmospheric turbulence is high.

  observe a weaker quasar close to the target source.

  check atmospheric phase monitor
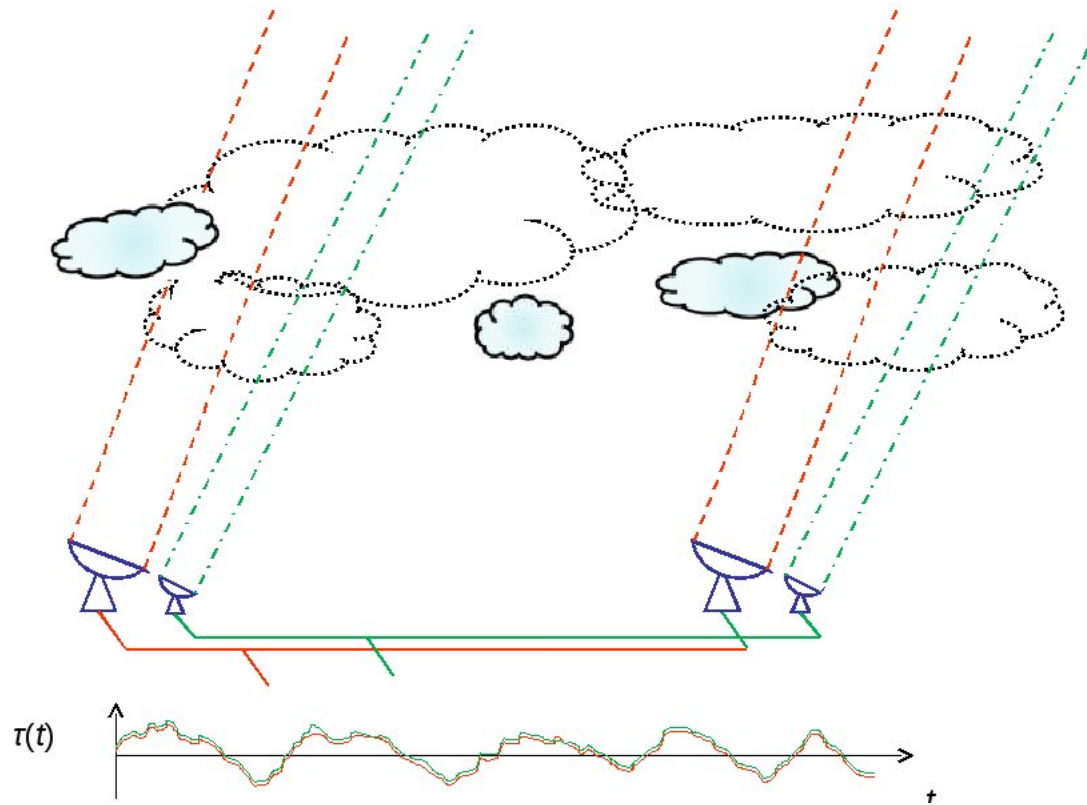
Figure 13: Paired Antenna Calibration System using 3.5 m antennas at 30 GHz. The 3.5 m antennas are paired with 6.1 and 10.4m antennas making science observations at millimeter wavelengths. The 3.5 m antennas simultaneously observe calibration sources in the 1 cm band. For calibration sources within a few degrees, the millimeter wavelength observations of the science target source, and the observations of the calibrator at 1cm, sample similar atmospheric phase fluctuations, allowing us to correct for the atmospheric phase fluctuations on long baselines at millimeter wavelengths. Thanks to Ashley Zauderer for this figure.

CARMA 2–5 and SZA 21–20
Calibrator 3C111 during 1mm Science Track
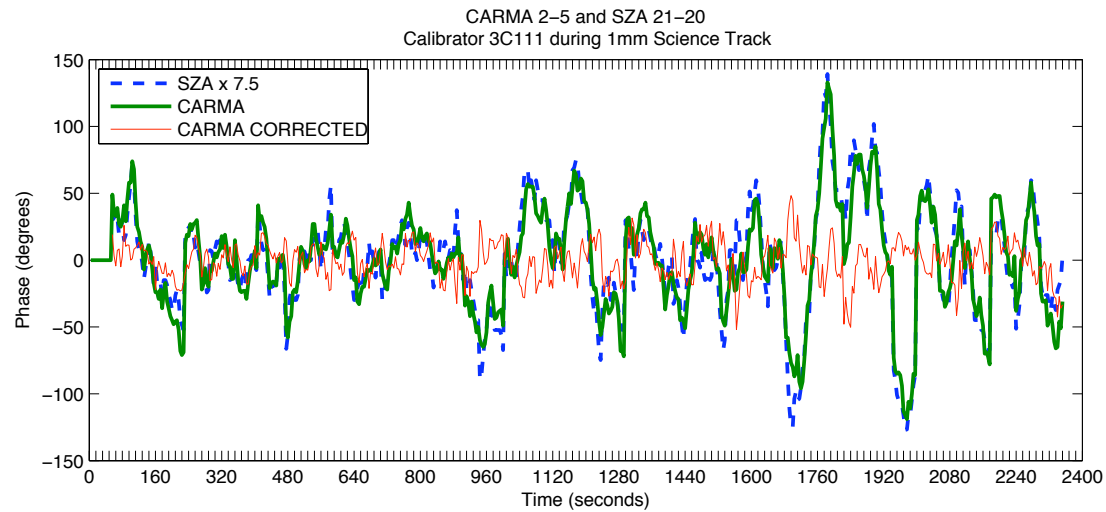
Figure 14: Phase correction using Paired Antenna Calibration System. The thick (green) line plots the phase versus time measured between CARMA antennas 2 and 5 while observing the radio source 3C111 at 225 GHz. The large phase fluctuations are caused by atmospheric turbulence on the long baseline between antennas 2 and 5. The dashed (blue) line plots the phase between two 3.5 m antennas which are close to CARMA antennas 2 and 5, but observing at 30 GHz. The 30 GHz phase multiplied by 7.5 (225/30), closely follows the 225 GHz phase allowing us to correct the 225 GHz phase. The thin (red) line shows the 225 GHz phase, corrected for atmospheric phase fluctuations. Thanks to Ashley Zauderer for this figure.
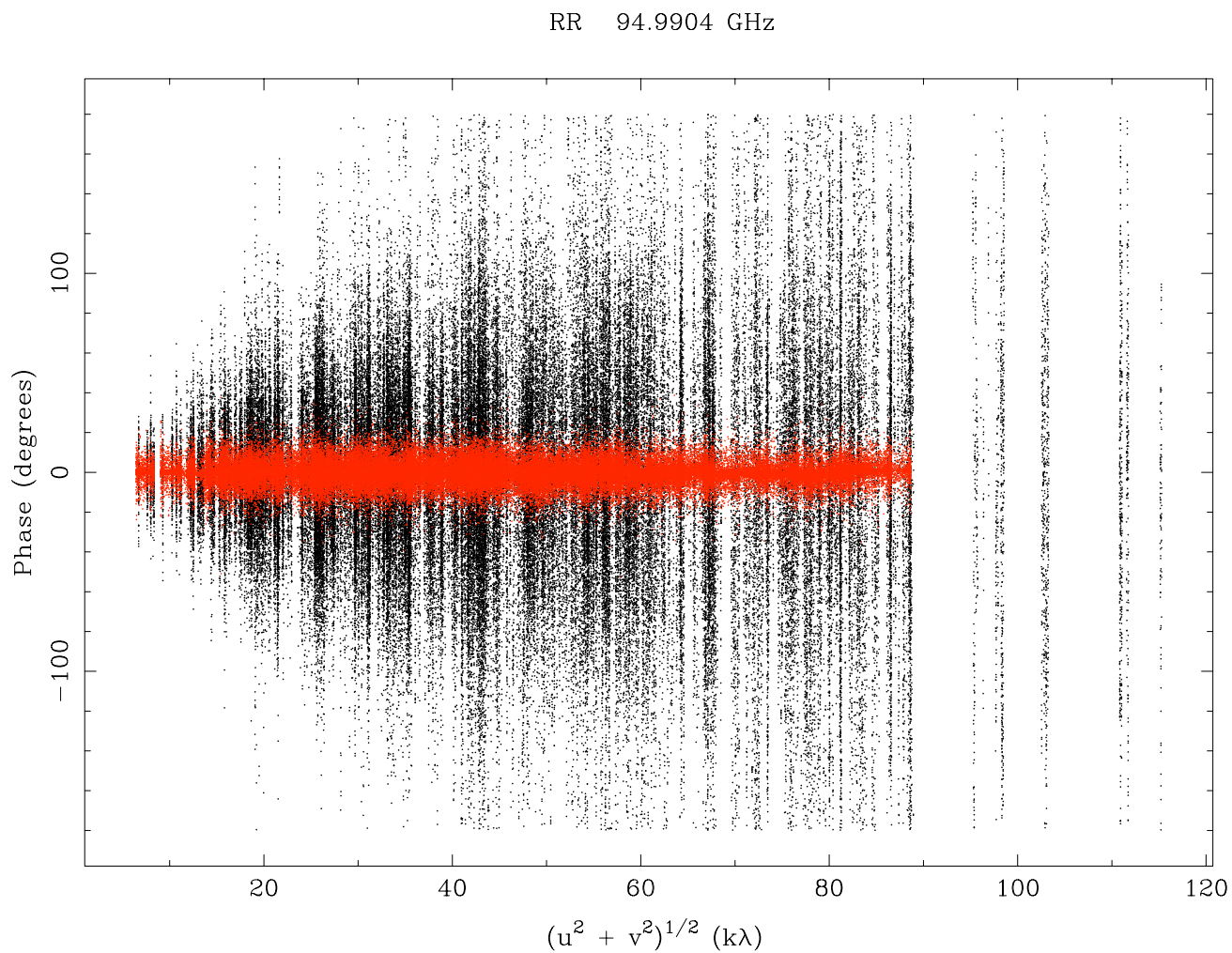
Figure 15: 3c454 before (black), and after (red) selfcal with interval=5min using antennas within $30k\lambda$ to reduce atmospheric phase fluctuations. Baselines longer than $\sim 90k\lambda$ do not have any antennas within $30k\lambda$, and hense are uncalibrated by the selfcal.Bandpass calibration used mfcal with interval=10 min

6.11 Baseline-based calibration

$$V'_{ij} = G_{ij}\,(t, f, p) \times V_{ij} + noise$$

$$Measured\ visibility = Gains \times True\ visibility + noise.$$

for a point source, V_{ij} = Flux density (Jy), so

$$G_{ij}\,(t, f, p) = V'_{ij} + noise$$

6.12 Antenna-based calibration - selfcal

$$G_{ij}\,(t, f, p) = g_i\,(t, f, p) \times g_j^*\,(t, f, p)$$

• Solve for $g_i\,(t)$ as a function of time only.

$$\chi^2 = \Sigma\,(V'_{ij} - g_i g_j^*\,V_{ij})^2 / \sigma_{ij}^2)$$

χ^2 sum over time interval, Δt.

selfcal can include:

– multiple frequency channels and pointings.

– planet models

– model images

– default is phase-only

6.13   Bandpass calibration - mfcal

$$G_{ij}\ (t, f, p) = g_i\ (t, f, p) \times g_j^*\ (t, f, p)$$
$$g_i\ (t, f, p) = g_i\ (t) \times g_i\ (f)$$

- Solve for antenna gains, $g_i(t)$ as a function of time.
- Solve for bandpass, $g_i\ (f)$, as a function of frequency.
- Solve for XX and YY, total intensity polarizations.

$$\chi^2 = \Sigma\ (V'_{ij} - g_i g_j^*\ V_{ij})^2/\sigma_{ij}^2)$$

6.14 Polarization calibration - gpcal

$$G_{ij}\,(t,f,p) = g_i\,(t,f,p) \times g_j^*\,(t,f,p)$$

$$g_i\,(t,p) = g_i\,(t) \times g_i\,(p)$$

$$\chi^2 = \Sigma\,(V'_{ij} - g_i g_j^*\,V_{ij})^2/\sigma_{ij}^2)$$

- Solve for antenna gains as a function of time, $g_i\,(t)$.
- Solve for instrumental polarization, $g_i\,(p)$.
- Solve for polarization leakage, and XY phase.
- Solve for source polarization if and YY total intensity polarizations.

6.15   Self calibration

• Solve for antenna gains as a function of time using a model image.

$$G_{ij}\,(t,f,p) = g_i\,(t,f,p) \times g_j^*\,(t,f,p)$$
$$\chi^2 = \Sigma\,(V_{ij}' - g_i g_j^*\,V_{ij})^2/\sigma_{ij}^2)$$

• Same algorithm as antenna-based calibration for point source.

• Use model image for true visibility, V_{ij} to solve for antenna gains, g_i.

• Make new image using these gains, deconvolve, and make new model.

• clip model image to exclude noise.

• Iterate to find model and gains consistent with measured visibilites and noise σ_{ij}.

6.16   Calibration Summary

- For each calibration, the error in the measured visibility is given by:

$$\delta V' = \delta G \times V + thermal\ noise$$

   V is the true source visibility and G is the calibration factor.

- The calibrations are themselves limited by thermal noise.

- Balance between time calibrating and time on target.

- Prefer random thermal noise rather than systemic calibration errors.

   for strong sources: work harder on calibration.

   for weak sources: better to spend more time integrating on the target source.

- Sensitivity for each baseline is given by:

$$\delta S = Jyperk \times Tsys/\sqrt{2\ B\ \Delta t}$$

Table 1: Sensitivity per baseline. Assuming 80% aperture efficiency, Tsys=200 K, with a 1 minute integration in a 4 GHz bandwidth with 1 MHz spectral resolution. For antenna based calibration, the RMS is reduced by $\sim \sqrt{(Nants)}$

Antennas	Equivalent diameter	JyperK	RMS (4 GHz)	RMS in 1 MHz	RMS in 5″
m x m	m	Jy/K	[mJy]	[Jy]	[K]
10.4 x 10.4	10.4	41	13	0.8	4
10.4 x 6.1	8.0	69	23	1.4	7
6.1 x 6.1	6.1	118	39	2.4	12
10.4 x 3.5	6.0	122	40	2.5	12
6.1 x 3.5	4.6	208	68	4.3	21
3.5 x 3.5	3.5	359	118	7.4	36

7   IMAGING

7.1   Imaging extended sources

- Review of basic math

- Brightness distribution is FT of sampled visibility data.

- We only have discrete samples of V, so we define a weighting function W, and evaluate:

$$I'(x,y) = \int W(u,v)V(u,v) \exp \frac{-2\pi i}{\lambda}(ux + vy)\, dudv$$

- The weighting function W can have any value where V is sampled,

  $W = 0$ where V is not sampled.

  I' is The Fourier transform of the product of V and W,

  which is the convolution of the Fourier transforms of V and W:

$$I'(x,y) = B(x,y) \star [I(x,y)A(x,y)]$$

  where

$$B(x,y) = \int W(u,v) \exp \frac{-2\pi i}{\lambda}(ux + vy)\, dudv$$

B is the synthesized beam.

7.2   Gridded Fast Fourier Transform

- In order to use a Fast Fourier Transform algorithm,

    we resample the (u,v) points onto a gridding u-v plane.

    uv-data are multiplied by the weighting function W,

    convolved by a function C,

    and resampled onto a regular grid by Π

$$[(V \times W) \star C] \times \Pi <= FFT => [(I \star B) \times c] \star \text{III}$$

- The Fourier transform of the gridded u-v data is an image of the sky brightness distribution I,

    convolved the synthesized beam B,

    multiplied by c,

    and convolved by III.

- The convolution by III replicates the image at intervals $1/\delta uv$,

    where δuv is the sample interval of the gridded u-v data.

- Aliasing in the sky brightness image is minimized by chosing a function C,

    so that its Fourier transform c falls to a small value at the edge of the image.

- The width of the image is $1/\delta uv$.

7.3   Image size and pixel sizes in sky plane and (u,v) plane

- image size and sample interval in the gridded (u,v) and the (x,y) sky plane
  are related through the Fast Fourier Transform.

$$Image\ size = N\ \delta xy = 1/\delta uv$$

$$(u,v)\ plane\ size = N\ \delta uv = 1/\delta xy$$

- choosing the pixel and image size.

  the image size, N and sample interval δxy are chosen in sky plane.

  x and y coordinates may be independently specified.

  the image size must be large enough to contain the FOV being imaged.

$$N\ \delta xy > field\ of\ view$$

- The (u,v) plane must be large enough to accomodate the sampled (u,v) data.

$$N\ \delta uv > 2 \times D_{max}/\lambda$$

- MIRIAD **invert**

  default $\delta xy = \sim \lambda/3D_{max} \sim 1.5 \times Nyquist$

  default $N\ \delta xy = Primary\ beam\ FWHM$

- Mosaicing **invert options=mosaic**

  image size, N, specifies subimage for each pointing

  image size, $N\ \delta xy = $ full width at 5% in primary beam (**pbplot**)

  smooth overlap between subimages for each pointing in mosaic image.

  imsize should not be a power of 2.

7.4 Spectral Line Imaging

- Use same beam for all frequency channels.

- Spectral line images are scaled by ν/ν_0

- Spectral channels can be averaged without interpolation.

- Use same beam for deconvolution.

$$I'(x, y, \nu) = B(x, y, \nu_0) \star [I(x, y, \nu)A(x, y, \nu_0)]$$

7.5 Bandwidth smearing and MFS imaging

- Wideband image is smeared in radial direction

$$\Delta r/r = \Delta\nu/\nu$$

- Multifrequency Imaging

  use spectral channels to make wideband image.

  each frequency channel is independent uv sample.

7.6 Deconvolution

- Fourier Transform is a linear operation. Deconvolution is not.

- CLEAN

    Hogbom, Clark, SDI, and MX algorithms

    iterative source subtraction from specified region of image

    removes sidelobes which are outside the region cleaned.

    converges when residual image is consistent with noise.

- RESTOR

    convolve the subtracted source model by Gaussian beam

    default: add the residual image

- MAXEN

    Maximum Entropy Deconvolution

    Maximize entropy, H, consistent with observations:

$$H = -\Sigma \ (I \ log(I/M \ e)$$

subject to constraint

$$\chi^2 = \Sigma \ (V' - V)^2/\sigma_{ij}^2$$

    Entropy measure: either "gull", -p log(p/e) or "cornwell", -log(cosh(p)

    I is the MEM image, M is a default image.

- MAXEN is a gradient search algorithm:

  convergence and behavior of MAXEN depends strongly on RMS.

  initial image model and total FLUX constraint also possible.

  - primary beam weight the current MEM image
  - FFT to get predicted visibility V' from image and beam .
  - accumulate χ^2
  - generate new MEM image.
  - iterate until MEM image is consistent with the data.

- MIRIAD **clean, maxen, uvmodel** handle spectral line image models

- Hybrids, a-priori models, uniqueness

  CLEAN is good for point sources.

  MEM is good for smooth, extended brightness distributions.

  MEM and CLEAN image models in units Jy/pixel

  UVMODEL subtracts image models from the uv-data.

  image model is consistent with the data. It is not unique.

7.7 Self Calibration

- Uses an image model to calibrate the uv-data.

  Solve for $g_i(t)$ as a function of time.

$$\chi^2 = \Sigma\ (V'_{ij} - g_i g_j^*\ V_{ij})^2/\sigma_{ij}^2)$$

- summed over time interval, Δt.

- MIRIAD **selfcal** handles spectral line image models:

  multiple frequency channels

  multiple pointing centers

  point source and planet models

7.8 Large Field Imaging

- arrays are good at mapping compact structures.

- single dishes are good at mapping large scale structure.

- telescopes are matched filters to a set of spatial scales.

- importance for getting correct answers for spectral index, etc;

- many astrophysical quantities are derived from ratios

  $^{13}CO/^{12}CO = I(^{13}CO) \star B(^{13}CO)/I^{12}CO) \star B(^{12}CO)$

  $SI = log[I(\nu_1) \star B(\nu_1)] - log[I(\nu_2)) \star B(\nu_2)]/[log(\nu_1) - log(\nu_2)]$

  WRONG answer, since a/b is not equal to $(a - a')/(b - b')$

  a' and b' are the missing large scale structure not sampled by an interferometer array

7.9   Short Spacing Problem

- interferometer array samples spacings from D_{min} to D_{max}.

    source structure with angular scale $> \lambda/2D_{min}$ is not sampled.

    shortest spacing $>$ dish diameter D, else collision or shadowing.

- importance for getting correct answers for spectral index, etc;

- negative sidelobes due to extended structure

- filling in missing spacings with larger single dish or Ekers-Rots scheme

- shortest spacings are partially sampled, then not at all less than some uvmin.

    uv-samples in annulus between uvmin and uvmax

    synthesized beam is a $J_1(x)/x$ for uvmax, minus a $J_1(x)/x$ for uvmin.

    this causes a negative basin around the source.

- shortest interferometer spacings, are a just few Fourier components

    i.e. sine waves, with quite high amplitudes.

    Images may look better without them.

    convolve the uv-plane inner edge to attenuate the few short spacings sampled by interferometer.

7.10 Sampling Short Spacings

- single dish observations

    single dish samples spacings from 0 to D_{ant}.

    interferometer array samples spacings from D_{min} to D_{max}.

    ideal single dish $D_{ant} \sim 2 \times D_{min}$

    need overlap for calibration.

- multiple beams for each antenna

    (Welch 1984, Granada IAU/URSI conference proceedings)

    illumination pattern rotates on sky for Alt-Az antennas.

    cross-talk between beams gives variable DC offsets.

- Heterogeneous antenna arrays.

    CARMA 10.4, 6.1 and 3.5m antennas.

    original MMA (ALMA) proposal was for 4m and 10m antennas.

- Mosaicing

    Ekers and Rots 1979, Groningen IAU

    Cornwell non-linear mosaicing using MEM

    Clean mosaic.

7.11 Single Dish Observations

- Single dish beam $A(x, y)$ convolves the sky brightness distribution $I(x, y)$

$$I'(x, y) = I(x, y) \star A(x, y) \times \Pi(x, y)$$

- Fourier transform gives the visibility data sampled in the uv-plane

$$V'(u, v) = V(u, v) \times a(u, v) \star \pi(u, v)$$

$a(u, v)$ is the weighting of spatial frequencies sampled by the single dish.

sampled visibilities are convolved by π, the Fourier transform of Π.

uv-data are aliased if $\pi < 2D_{ant}/\lambda$

sample single dish observations with $\Pi < \lambda/2D_{ant}$ to avoid aliasing.

7.12 Combining Single Dish and Interferometer Observations

- single dish samples spacings from 0 to D_{ant}.

  zero spacing gives the total flux in the image

- interferometer array samples spacings from D_{min} to D_{max}.

- ideal single dish $D_{ant} \sim 2 \times D_{min}$

  need overlap for calibration.

- IMMERGE linearly merges single dish and interferometer images.

  deconvolve single dish observations. Need single dish beam.

  multiply by interferometer image primary beam pattern.

  sample overlapping uv-data in an annulus.

  establish consistent calibration between single dish and interferometer.

  merge the two images together

- MOSAIC joint deconvolution of a mosaic and single dish image.

- MOSAIC using the single dish image as a default image.

7.13   Ekers and Rots

- Mosaic observations measure a range of visibilities around each (u,v) point.

   two antennas, diameter D, separated by d, sample the wavefront between d-D and d+D

- Measure visibility at pointing center s'

$$V(u, s') = \int I(s)A(s - s') \exp \frac{2\pi i}{\lambda} usds$$

- Phase gradient across aperture correlates different spacings on antenna surface.

- Observing a grid of pointings measures different Fourier samples of wavefront.

- Fourier transform w.r.t. pointing measures visibilities around each (u,v) point.

$$V(u, u') = a(u') \times \int I(s)A(s - s') \exp \frac{2\pi i}{\lambda}(u + u')sds$$

$$V(u, u') = a(u') \times V(u + u')$$

- In practice we recover $\sim D/2\lambda$ around each (u,v) sample.

   i.e. uv-tracks are $\sim D/\lambda$ wide, multipled by $a(u')$

- Need single dish observations to sample $<\sim D/2\lambda$ with good SNR.

8 MOSAIC IMAGES

8.1 Astronomical Requirements

- Millimeter wavelength Imaging from Comets to Cosmology

    Hale Bopp 1 AU 3 arcmin 0.1 arcsec (75 km)

    Orion Core 500 pc 40 arcsec 0.1 arcsec (50 AU)

    Cas A 3 kpc 5 arcmin 1 arcsec (3000 AU)

    IC342 nucleus 2 Mpc 1 arcmin 1 arcsec (10 pc)

    Cygnus A 200 Mpc 3 arcmin 1 arcsec (1 kpc)

    Cluster Core 2 Gpc 3 arcmin 10 arcsec (100 kpc)

- Field of View > Primary beam width ($\sim$ 1 arcmin at λ 3mm)

- Resolution < $\sim$ 1 arcsec.

- Spatial dynamic range $\sim$ 1000.

8.2 Heterogeneous arrays

- for extended sources we need to correct for the primary beam pattern.

- sky is illuminated by the antenna voltage patterns for each pair of antennas.

  for each antenna pair (i, j),

  $$P_{i,j}(\mathbf{s}) = V_i(\mathbf{s}) \times V_j^\star(\mathbf{s})$$

  primary beam patterns depend on the aperture illumination.

- CARMA primary beams from 6.1 x 6.1, 10.4 x 10.4, and 6.1 x 10.4

- ALL CARMA images are mosaics – even with only 1 pointing center.

- mosaicing algorithms clip primary beam at $\sim 5\%$ level,

  avoids uncertainties in primary beam at low levels.

  within 5% level, primary beam pattern $\sim$ Gaussian.

8.3 Primary Beam Calibration

- Primary beam pattern for each pair of antenna types.

- Same pointing pattern for all antennas reduces number of primary beam types and minimizes primary beam errors.

- Mosaic observations with 10.4, 6.1 and 3.5 m antennas produce 6 primary beam types at each pointing center.

- Primary beam is the product of voltage patterns for each antenna pair.

- Complex valued PB if voltage patterns are not identical.

- Primary beam errors degrade the image fidelity.

- If the pointing centers are offset, there are uncertainties in the resulting product of voltage patterns, and the asymmetric primary beam patterns rotate on the sky.

- For mosaic observations we would need to calculate a primary beam for each pointing, baseline, and integration. Whilst this is possible in principal, the computing burden is substantial, and errors in the visibility data are hard to measure.

- In order to keep the number and parameterization of the primary beam models manageable, the most convenient way to make mosaicing observations is to use the same pointing pattern for all antennas at the sample interval required for the largest antenna in the sub-array being used.

8.4 Mosaicing Algorithms

- Two problems:
    1. Mapping a large Field of view.
    2. Imaging large scale structures.

8.5 Mapping Field of view larger than primary beam

.

- same as single dish mapping

- scan antennas across the source and sample sky at Nyquist

- Primary beams $A(x, y)$ convolve the sky brightness distribution $I(x, y)$
    sampled at intervals $\delta\theta$ by Π
$$I'(x, y) = I(x, y) \star A(x, y) \times \Pi(x, y)$$

- Fourier transform gives the visibility data sampled in the uv-plane

$$V'(u, v) = V(u, v) \times a(u, v) \star \pi(u, v)$$

    $a(u, v)$ is the weighting of spatial frequencies sampled by the primary beams.
    sampled visibilities are convolved by π, the Fourier transform of Π.
    uv-data are aliased if $\pi < 2D_{ant}/\lambda$
    sample antenna pointings with $\delta\theta < \lambda/2D_{ant}$ to avoid aliasing uv-data.

8.6 Imaging large scale structures

• Interferometer data image $I'(x, y)$

$$I'(x, y) = \int W(u, v) V(u, v) \exp \frac{-2\pi i}{\lambda} (ux + vy) \, du dv$$

$$I'(x, y) = I(x, y) \times A(x, y) \star B(x, y)$$

• in Fourier plane the measured visibility $V'(u, v)$ is:

$$V'(u, v) = V(u, v) \star a(u, v) \times W(u, v)$$

$W(u, v)$ is the sampling in the uv-plane.

$a(u, v)$ is the weighting of spatial frequencies sampled by the antennas.

image is convolved by $B(x, y)$.

image is aliased if $\delta uv > D_{ant}/2\lambda$.

sample uv-data $\delta uv < D_{ant}/2\lambda$ to avoid aliasing in sky plane.

8.7 Linear Mosaicing Algorithms

- linear mosaic is primary beam weighted linear combination of pointings.

$$I'(x) = g(x)\Sigma \ (A(x - x_i) \ I_i(x)/\sigma_i^2)/(\Sigma \ A^2(x - x_i)/\sigma_i^2)$$

- MIRIAD **invert options=mosaic** – just like single field imaging.

- $g(x)$ is residual primary beam pattern to keep noise constant across mosaic image

- synthesized beam is different for each pointing.

  synthesized beam has $Npts$ image planes.

- sidelobes $\sim 1/Npts$

- pointing errors may be common to adjacent pointings

- gain and phase errors may be common to adjacent pointings

- observing strategy is to sample all pointings in short time interval.

- selfcal can be used with multiple pointing centers.

8.8   Maximum Entropy Mosaic Deconvolution

- Maximize entropy, H, consistent with observations:

$$H = -\Sigma \ I \ log(I/M \ e)$$

subject to χ^2 constraint summed over all pointings (x', y')

$$\chi^2 = \Sigma \ (V'(u, v, x', y') - V(u, v, x', y'))^2 / \sigma(u, v, x', y')^2$$

- Entropy measure: either "gull" (-p log(p/e)) or "cornwell" (-log(cosh(p))

- I is the MEM image, M is a default image.

- can do joint deconvolution of a mosaic and single dish image.

- can use single dish image as a default image.

- convergence and behavior of MOSMEM depends strongly on RMS.

- initial image model and total FLUX constraint also possible.

- gradient search algorithm:
  - primary beam weight the current MEM image
  - FFT to get predicted visibility V' from image and beam .
  - accumulate χ^2 over all pointings (x', y')
  - generate new MEM image.
  - iterate until MEM image is consistent with the data.

- Maximum Entropy deconvolution pionered by Tim Cornwell

  find image which is consistent with all the data.

  may be many such images, so chose the most likely one.

  Maximum Entropy image subject to χ^2 constraints.

  gradient search algorithm in MEM and χ^2 image.

- MIRIAD uses an efficient user-friendly algorithm pionered by Bob Sault.

- MIRIAD **mosmem and mossdi** are like MAXEN and CLEAN for single field deconvolution.

- both algorithms start with images, not uv-data.

8.9　Sampling Requirements

- Sampling rates are set by both 10m and 6m antennas.

- Nyquist sample interval for uv data, $\delta uv = D_{ant}/2\lambda$.

- Nyquist sample interval for pointings, $\delta\theta = \lambda/2D_{ant}$.

- The number of pointings, $Npts \sim \Omega/(\delta\theta)^2$.

- Nyquist sample rate $\sim baseline/\lambda \times (2D_{10m}/\lambda)^2 \times 2\lambda/D_{6m} \times \Omega \times sdot$,

    D_{ant} is antenna diameter, Ω, source size, and $sdot = 2\pi/24/3600$).

    sample rate $= \sim (100m/\lambda) \times 2\lambda/6m \times Npts \times 7.2710^{-5}$

    Nyquist sample interval $\sim 400/Npts$ seconds

- The uv data oversampled by the larger antenna,

- pointing is oversampled by the smaller antenna.

- No loss in sensitivity; the oversampled data are accounted for.

- 10m antennas on long baselines for better SNR and reduce uv data sample rate.

- sample rate $= baseline/\lambda \times 2\lambda/D_{ant} \times \Omega/(\lambda/2D_{ant})^2 \times sdot$

    Larger antennas must sample faster.

    On-the-fly mosaicing needed for ALMA.

8.10 Image Fidelity as a Function of Source Size

- CARMA array can image $\sim 32''$ diameter with a single pointing center using the 15-antenna D-configuration at 230 GHz. must treat as mosaic observation.

- up to $\sim 64''$ diameter can be imaged with a 7-pointing hexagonal mosaic using the 15-antenna D-configuration at 230 GHz.

- image fidelity decreases as the source size increases.

- joint deconvolution gives the best image fidelity.

- image fidelity very dependent on high quality single dish data.

- default image for lower quality single dish data.

- fidelity improved by mosaic with 23-antenna DZ configuration.

  short spacings with 3.5m antennas sample large scale structure.

  and cross calibrate single dish and interferometer observations.

- CARMA memo 38

8.11 Flux and Brightness Sensitivity

• Single pointing

$\Omega_{source} < \Omega_{beam}$

Flux sensitivity

For N antenna array, total observing time $= N(N-1) \times t$

$$\Delta S = 2k/\eta A \times T_{sys}/\sqrt{(2\ B\ t)}$$

$$\Delta S \sim 2kT_{sys}/\sqrt{(2\ B\ t)} \times (1/\eta N D_{ant}^2) \sim 1/N D_{ant}^2$$

Brightness sensitivity

$$S = 2k\ T_b/\lambda^2 \times \Omega_{synth}$$

$$\Delta T_b = T_{sys}/\sqrt{(2\ B\ t)} \times (1/\eta N D_{ant}^2) \times \lambda^2/\Omega_{synth}$$

brightness temperature sensitivity is scaled up by beam filling factor:

$\Omega_{synth} \sim (\lambda/D_{max})^2$ and $\Omega_{beam} \sim (\lambda/D_{ant})^2$

$$\Delta T_b = T_{sys}/\sqrt{(2\ B\ t)} \times 1/\eta N \times (D_{max}/D_{ant})^2$$

$$\Delta T_b = T_{sys}/\sqrt{(2\ B\ t)} \times 1/\eta N \times (\Omega_{beam}/\Omega_{synth})$$

8.12 Mosaicing Sensitivity

$\Omega_{source} > \Omega_{beam}$

number of pointings $= \Omega_{source}/\Omega_{beam}$

observing time per pointing $= t \times (\Omega_{source}/\Omega_{beam})$

Flux sensitivity

$$\Delta S = 2k/\eta A \times T_{sys}/\sqrt{(2\ B\ t)} \times (\Omega_{source}/\Omega_{beam})^{1/2}$$

$\Omega_{beam} \sim (\lambda/D_{ant})^2;\ A \sim N D_{ant}^2$

$$\Delta S \sim 2k T_{sys}/\sqrt{(2\ B\ t)} \times (\Omega_{source}^{1/2}/\eta N \lambda D_{ant}) \sim 1/N D_{ant}$$

Brightness sensitivity

$$S = 2k\ T_b/\lambda^2 \times \Omega_{synth}$$

$$\Delta T_b = T_{sys}/\sqrt{(2\ B\ t)} \times 1/\eta N D_{ant} \times \lambda/\Omega_{source}^{1/2}$$

8.13 Hexagonal pointing grids

- pointing grids must sample the source

- easy to build custom grids using hexagonal patterns

- hexagonal grid sampled at Nyquist spacing $\lambda/2D_{ant}$

  oversampling by $\sqrt{(3)}/2$ helps the mosaicing process

  less time per pointing, but no loss in sensitivity

- MIRIAD tasks: **hex, hexc**

- Mosaicing simulations in $MIR/demo/carma – hex7.csh

8.14 Primary beam and Image sensitivity

- **IMLIST options=mosaic** List the mosaic table for an image.

- MOSSEN determines the rms and gain of a mosaiced image. Both of these parameters are a function of position (and also mildly frequency dependent).

  To avoid noise amplification at the edge of mosaiced regions, Miriad does not normally totally correct for the primary beam beyond a certain point.

- MOSPSF determines the point spread function for a linear mosaic produced by **invert options=mosaic**.

  Strictly speaking, the PSF varies with position and frequency. However if the pointing grid is fairly complete and the individual synthesized beam patterns are similar, the PSF is reasonably independent of position. It is also usually a good approximation that it is independent of frequency.

- DEMOS multiplies model of the sky primary beam paterns at a number of different pointing centers. It produces a different output for each pointing center. Thus this task performs the inverse of mosaicing. The input pointing centers and the primary beam size are indirectly specified by a visibility dataset.

  Because the outputs of DEMOS have primary beams applied, they can be used for comparison with visibility data and uncorrected images. In particular SELFCAL cannot handle a model which is primary beam corrected, though it can handle a visibility data file containing multiple pointings. Thus you could use DEMOS to break the model into several models which are not primary beam corrected.

9 Deconvolving Primary Beam Patterns from Mosaic Images

- An aperture synthesis array samples the cross correlation of the signals from an array of antennas.

- The signal from each antenna measures the sky brightness distribution weighted by the voltage pattern of the antenna.

- The usual assumption is that the illumination of the sky by the antenna beam pattern is invariant, and the same for all antennas, then an image of the primary beam weighted sky brightness can be formed from a Fourier transform of the measured cross correlations. Sources larger than the primary beam require a mosaic of interferometer and single dish observations at multiple pointing centers.

- If the primary beam is time variable, non axi-symmetric and different on each antenna, images can be deconvolved by subtracting a primary beam weighted model from the uvdata (CARMA memo 43).

10   DATA ANALYSIS

10.1   uv-data and images are complementary.

- uv-data are the observional data but hard to interpret
    uv-data can be compared with model brightness distributions.

- images are derived data products but easier to interpret

10.2   Fitting uv-data.

- UVFIT for point, disk, gaussian, shell or ring models
    needs initial estimates of source parameters.

- UVAMP plot uv-data in annuli versus uvdist.

10.3   Fitting images

- IMPLOT, CGDISP are the primary plotting tasks for images.

- ELLINT integrates an image in elliptical annuli.

- IMFIT fits point, disk, gaussian or beam objects to an image.
    needs initial estimates of source parameters.

- VELPLOT analyse spectra, position-velocity, and integrated velocity maps.

10.4 Comparing uv-data with images

- UVMODEL compares uv-data with an image model.

  the model can add, subtract, multiple, divide or replace the uv-data.

  can also process mosaic and polarization data.

10.5 Position Fitting

- use uvfit or imfit

- interferometer phase gives the position. Phase $\sim$ transit time.

- measured position is w.r.t. reference frame of calibration sources.

  use a set of reference sources around target source.

- fringe phase 2π ambibuity elliminated by multiple antenna separations.

- accuracy $\sim 1/SNR \times \lambda/D_{max}$, where SNR is the signal-to-noise.

  interferometer phase $= \frac{2\pi}{\lambda}\,\mathbf{b}.\mathbf{s}$

  $\mathbf{b}$ is antenna baseline. $\mathbf{s}$ is the source position

  measured phase $= \frac{2\pi}{\lambda}\,(\mathbf{b}.\mathbf{\Delta s} + \mathbf{\Delta b}.(\mathbf{s} - \mathbf{s_0}))$

  $\mathbf{\Delta s}$ is the estimated position offset of the target.

  $\mathbf{\Delta b}$ is the error in the antenna separation.

  $\mathbf{s} - \mathbf{s_0}$ is the angle between the target and weighted mean for reference objects.

11 CARMA HARDWARE - I. Receivers and Calibration (Dick)

- system block diagram; receiver, cal load, local osc, phaselocks, fiber, downconverter, correlator

- energy collected if observing 20 Jy source for 1 yr; would need to observe for 100,000 years to heat 1 drop of water by 1 C

- receiver types:

- bolometers: not suitable for interferometry because they don't preserve phase

- HEMT amplifiers: not yet competitive at 1mm

- heterodyne rcvr: downconvert to lower freq in a nonlinear device

- SIS mixers: photon-assisted tunneling; not a Josephson effect

- cryogenics; closed-cycle refrigerators, compressors

- local oscillator: Gunn oscillator

- must be synchronized between all antennas; discuss in lecture 2

- both USB and LSB are downconverted to IF; can be separated with 90 degree phase switch; also defer to lecture 2

- combining LO and signal: mylar beamsplitter

- receiver and system temperature

- calibration:

- ideally, calibrate on loads outside the earth's atmosphere

- the chopper wheel method

- CARMA sensitivity calculator

12 CARMA HARDWARE - II. Correlator; Software Control (Dave Hawkins)

– review system block diagram

– correlator is detector and spectrometer for the array

– XF vs FX

– delays, 2nd LO lobe rotation, sideband separation

– correlator modes

– FPGA's

– noise source

– system architecture

– Correlator Tour (Dave Hawkins)

13 CARMA SOFTWARE SYSTEM I (Marc)

– Intro to CARMA computers.

– Computers, control and monitoriing, data flow, archiving

– basic observing procedures, on-line monitors and data inspection

– key programs: sac, checksource, checkcat, checksafe (E array)

– Basic demos (students guided by Nikolaus)

– observe a point source (maser or quasar) and a planet.

– plot amplitude and phase vs. uvdistance

– constant amplitude for point source, Bessel function (with phase flips) for planet

– set up correlator in various modes, take spectra of Orion

14 CARMA SOFTWARE SYSTEM II (Marc)

– What software does an observatory need?

– Timekeeping

– Antenna and device control

– Monitor system (a.k.a. telemetry)

– Interprocess communication

– Data pipelines

– User interface

15 CARMA HARDWARE -III - local oscillators, phaselocks (Dick)

– Review system block diagram, heterodyne system, local oscillator

– Independent oscillators, 100 GHz, synchronized to fraction of one cycle over periods of hours (sounds hard)

– Basic phaselock: mix with reference, low pass filter, generate correction voltage; keeps phase relationship fixed

– CARMA phaselock chain; synthesizer, YIG, Gunn, 10 MHz, 50 MHz

– Fiber system; linelength correction

– Lobe rotation compute differential doppler shift due to earth's rotation for 100 GHz signal incident on 2 antennas 10-m apart: 0.24 Hz

– lobe rotators

– interferometer response for a double sideband conversion system

– need to offset freq of 1st LO as well as insert delays can be understood as removing differential doppler shift due to earth's rotation

– Phaselocks; the LO system

– Cable length measurement system

– Phase switching; Walsh functions

– Sideband separation by phase switching; note that only signals common to an antenna pair can be separated; noise appears in both sidebands

– Fiber optic hardware

– review system block diagram

16 ARRAY RECONFIGURATION (Nikolaus)

– moving the antennas and calibrating a new array configuration

– finding new pad coordinates

– finding pointing offsets.

– finding the delay centers

– radio and optical pointing

– finding a baseline

17   INTRODUCTION TO SINGLE DISH OBSERVING (Marc)

- Autocorrelation

- Position switching

- Computing the source spectrum

- Baseline (continuum) subtraction

- Efficiency improvements

17.1   Holography

- Antenna Voltage pattern

  antenna forms a weighted vector average of the E-field across the aperture

  $$V(\mathbf{s}) = \int W(\mathbf{r})\ E(\mathbf{r})\ \exp(2\pi i\ \mathbf{r}.\mathbf{s}/\lambda)\ \delta A$$

- We can measure the amplitude and phase of the voltage pattern by scanning one antenna across a strong radio source, or a radio transmitter, while using another antenna as a phase reference.

- The E-field distribution across the aperture is the Fourier transform of the Voltage pattern

  $$W(\mathbf{r})\ E(\mathbf{r}) = \int V(\mathbf{s})\ \exp(-2\pi\ i\ \mathbf{r}.\mathbf{s}/\lambda)\ \delta \mathbf{s}$$

- The measured aperture distribution gives the illumination - the weighting of the E-field - across the aperture. The phase gives the surface error.

  With sufficient resolution, we can clearly see the shadow of the feed legs and subreflector (FIGURE).

  Phase gradient across the aperture is due to pointing error.

- After removing the phase gradient and a quadratic term due to focus error, we measure a surface RMS ~ 30 microns in ideal conditions. These are very good antennas at millimeter wavelengths.

18   CARMA FUTURE PLANS

- polarization measurements
  - interferometer response LR, RL, etc in terms of Stokes parameters
  - Walsh function polarization switching schemes
  - polarization leakage terms and how to solve for them
  - mapping procedures

- Atmospheric phase fluctuations and what we plan to do about them
  - like floppy backup structure on a big telescope
  - causes decorrelation, ruins aperture efficiency
  - show results at long and short baselines
  - phase structure function

- PACS – Paired Antenna Calibration System using 3.5m antennas.

- Rapid switching; put calibrator in grid file;
  - observe weak nearby calibrator often, strong faraway calibrator less often

- calibrating by observing the total power; need for extreme gain stability; typical results

- 1 cm system

- wideband receivers

- 23-antenna CARMA array

19 Imaging Simulations with CARMA-23

- spacings between 3.5 and 6.1 m sampled by the 3.5 m antennas provide better quality data for these short spatial frequencies, than can be obtained from the joint deconvolution with the 10.4 m single dish data.

- different antenna diameters allow a larger range of spatial frequencies to be sampled by interferometer observations.

- different primary beam patterns decouple source brightness distribution from primary beam illumination.

- central hole in the uv sampling is smaller; less information which depends on single dish observations.

- large region of overlap in spatial frequencies used to cross calibrate single dish and interferometer observations.

- heterogeneous interferometer observations provide excellent cross calibration of the 3.5, 6.1 and 10.4 m antennas.

- 3.5 m antennas effectively sample a guard band around the source brightness distribution; this helps the mosaicing algorithms to define the extent of the source. These observations of a guard band without having to make observations at extra pointing centers is a bonus.
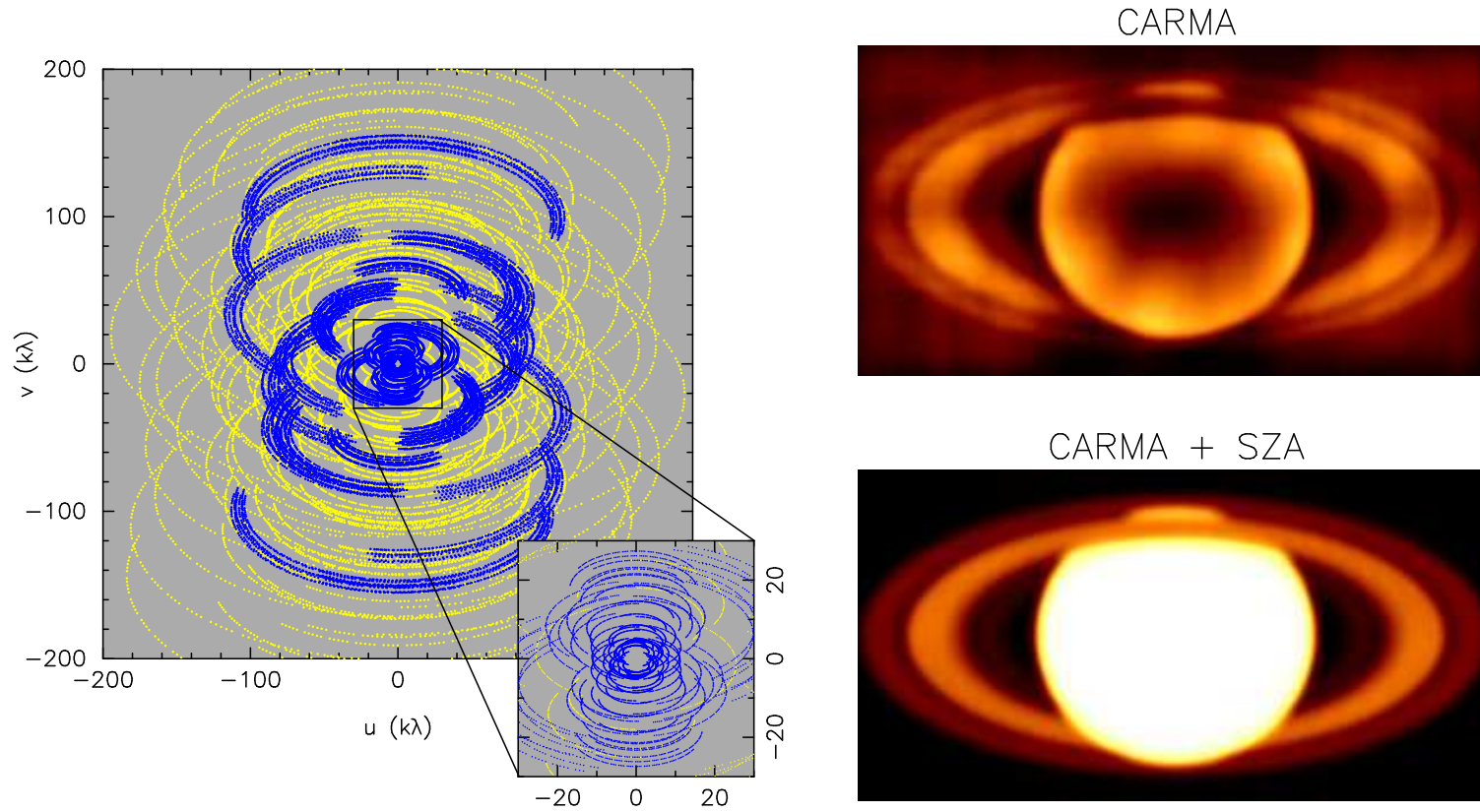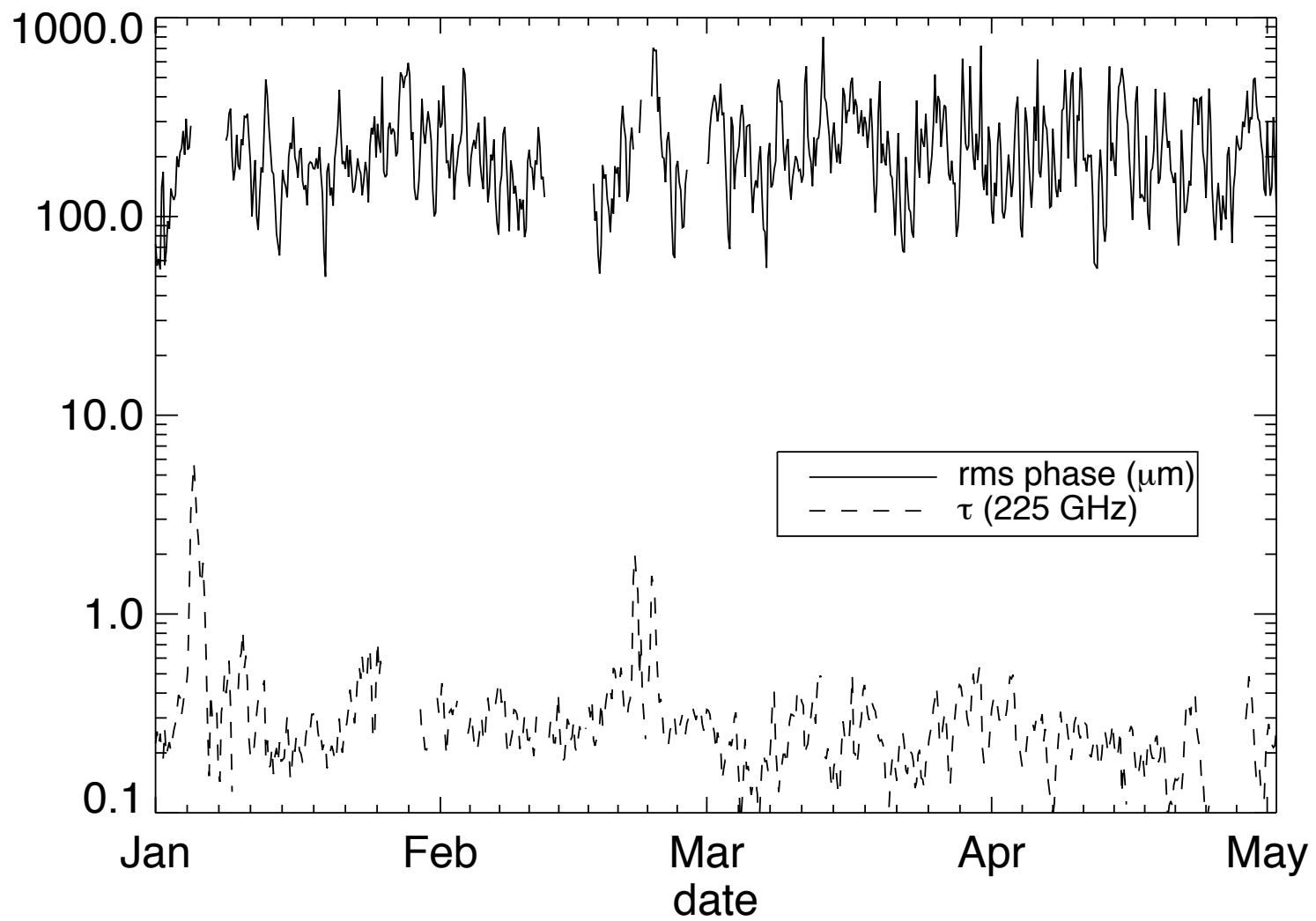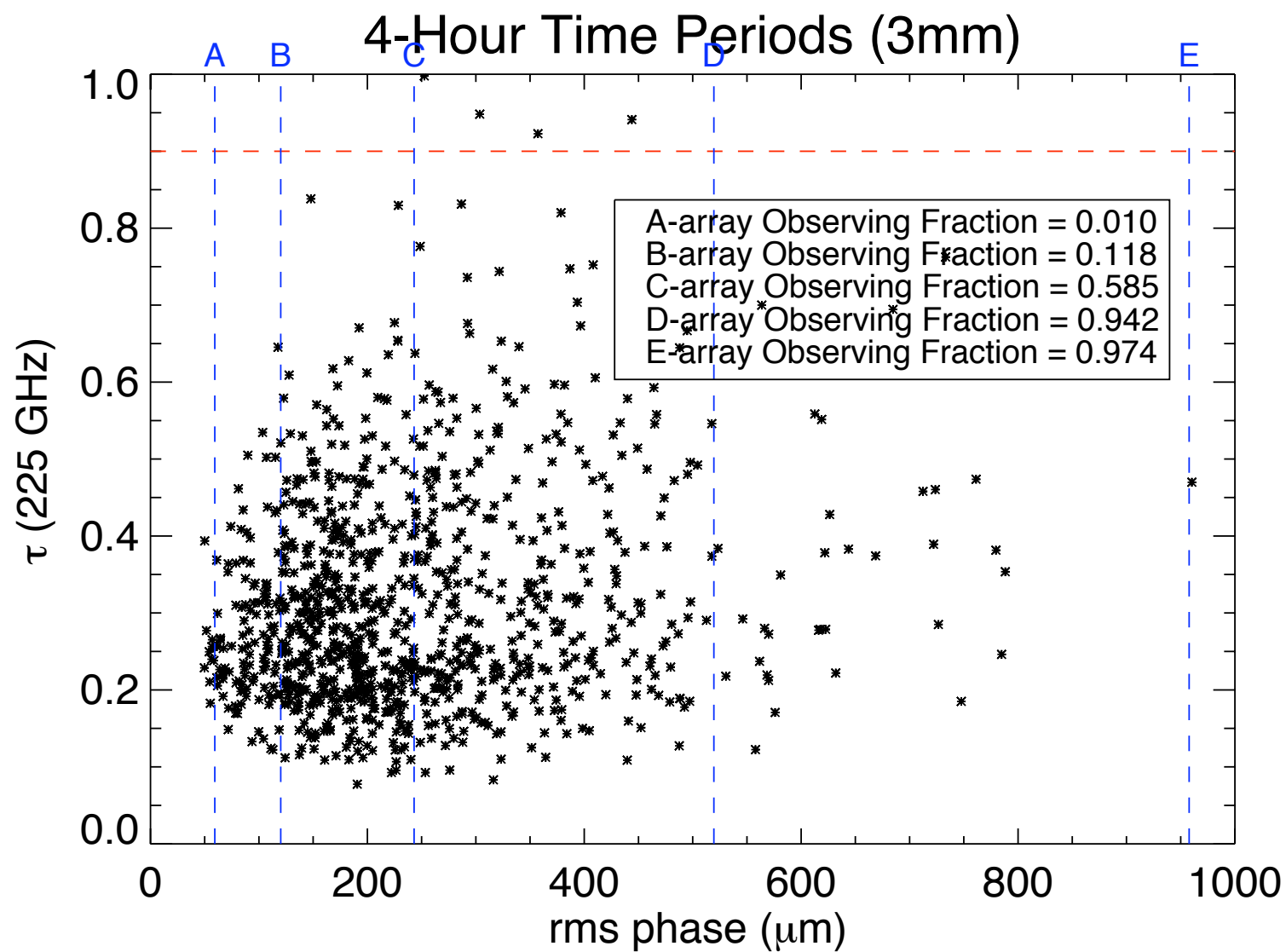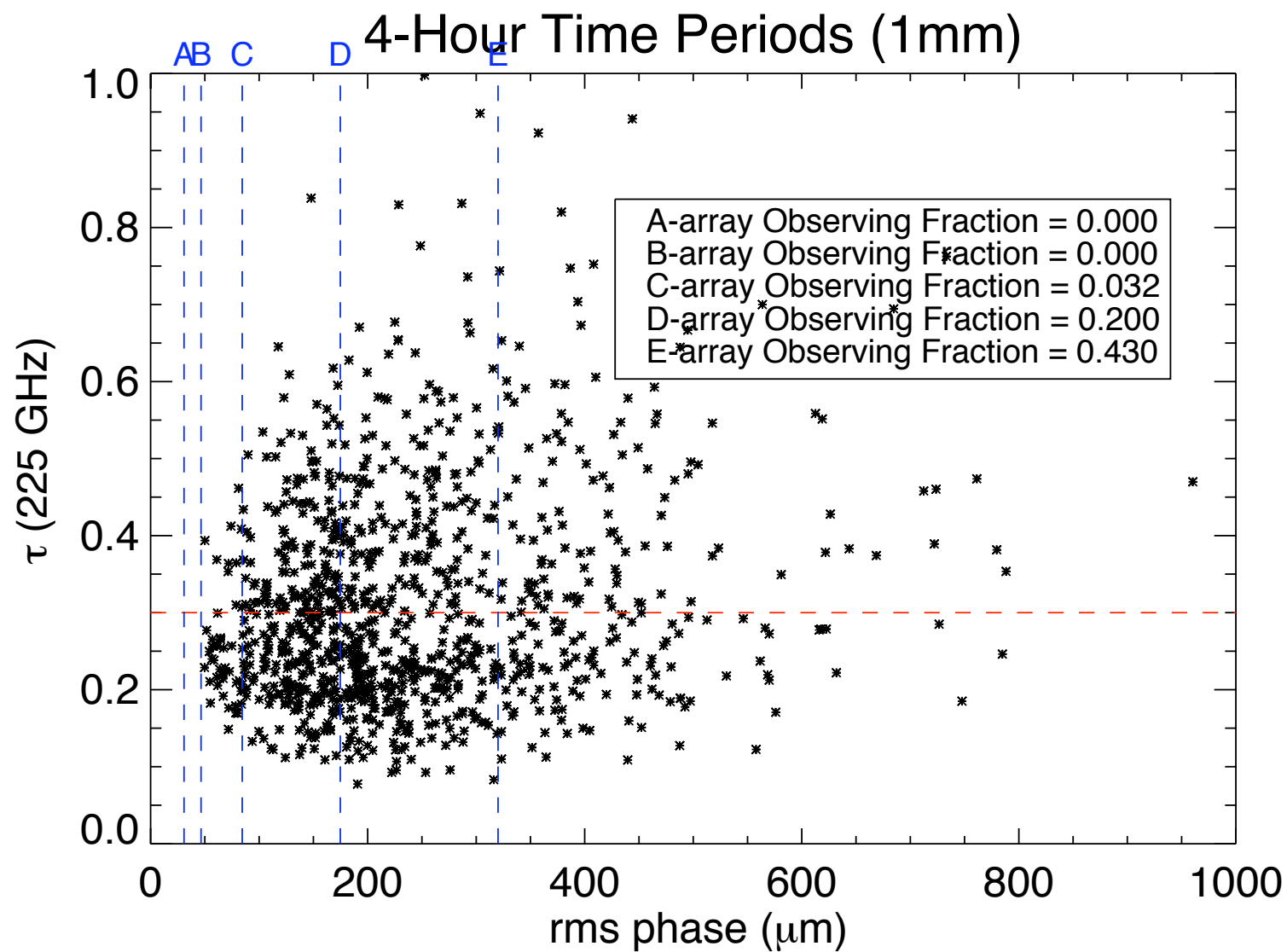
Figure 16: CARMA 23-element heterogeneous array. Left: uv data sampling at 100 GHz , DEC=30 . Yellow points: uv coverage for the CARMA 15-element array; blue points show the additional uv coverage when the 3.5-m antennas are used in the 23-element array. The dense uv sampling at short spacings shown in the inset, gives sensitivity to larger scale structure. Right: Simulated CARMA observations of Saturn show the increase in image fidelity for extended sources provided by the 3.5 m antennas.

2008 4-Hour Time Periods

4-Hour Time Periods (3mm)

A-array Observing Fraction = 0.010
B-array Observing Fraction = 0.118
C-array Observing Fraction = 0.585
D-array Observing Fraction = 0.942
E-array Observing Fraction = 0.974

τ (225 GHz)

rms phase (μm)

4-Hour Time Periods (1mm)

A-array Observing Fraction = 0.000
B-array Observing Fraction = 0.000
C-array Observing Fraction = 0.032
D-array Observing Fraction = 0.200
E-array Observing Fraction = 0.430

τ (225 GHz)

rms phase (μm)

ACKNOWLEDGMENTS

References

BIMA memo 45, 1999, *BIMA Array response to extended structure*, M.C.H. Wright, http://bima.astro.umd.edu/memo/memo

BIMA memo 73, 1999, *Image Fidelity*, M.C.H. Wright, http://bima.astro.umd.edu/memo/memo.html

CARMA memo 5, 2002, *Compact Configuration Evaluation for CARMA*, Melvyn Wright.

CARMA memo 19, 2004, *Version 1 CARMA Configurations for Cedar Flat*, Tamera Helfer and Melvyn Wright.

CARMA memo 20, 2004, *Version 2 CARMA Configurations for Cedar Flat*, Tamera Helfer.

CARMA memo 25, 2004, *SZA location at CARMA site*, Melvyn Wright.

CARMA memo 38, 2007, *Image Fidelity as a Function of Source Size and Calibration Errors*, Melvyn Wright.

CARMA memo 43, 2008, *Deconvolving Primary Beam Patterns from Mosaic and Polarization Images*, Melvyn Wright & Stuartt Corder.

Cornwell, T.J., Holdaway, M.A. & Uson, J.M., 1993, *Radio-interferometric imaging of very large objects: implications for array design*, A&A 271, 697.

Dunn, D.E., de Pater, I., Wright, M., Hogerheijde, M., and Molnar, L.A., 2005, *High Quality BIMA/OVRO Images of Saturn and its Rings at 1.3 and 3 mm* AJ, 129,1109

Ekers, R. D., & Rots, A.H. 1979, in IAU Col. 49, *Image Formation from Coherence Functions in Astronomy* , ed. van Schooneveld, C. (Dordrecht:Reidel), p.61

Holdaway, M. A., 1998, *Mosaicing with Interferometer Arrays*, Synthesis Imaging in Radio Astronomy II, ASP Conference Series, G. B. Taylor, C. L. Carilli and R. A. Perley (Eds)

Holdaway. M.A., 1999, *Mosaicing with Interferometer Arrays*, ASP Conference series 180, 401.

Nijboer, R. J., Noordam, J. E., 2005, *LOFAR Calibration*, Astronomical Data Analysis Software and Systems XVI ASP Conference Series, Vol. 376, 237, Richard A. Shaw, Frank Hill and David J. Bell. (Eds)

Nijboer, R. J., Noordam, J. E., Yatawatta, S. B., 2006, *LOFAR Self-Calibration using a Local Sky Model*, Astronomical Data Analysis Software and Systems XV ASP Conference Series, Vol. 351, 291, Carlos Gabriel, Christophe Arviset, Daniel Ponz, and Enrique Solano. (Eds)

SKA memo 103, 2008, *Deconvolving Primary Beam Patterns from SKA Images*, Melvyn Wright & Stuartt Corder.

Sault, R.J., Staveley-Smith, L & Brouw, W.N., 1996, *An approach to interferometric mosaicing*, A&A Supp., 120, 375

Bob Sault & Neil Killeen, 2006, *Miriad Users Guide*, http://www.atnf.csiro.au/computing/software/miriad